

## Modeling soil thermal and carbon dynamics of a fire chronosequence in interior Alaska

Q. Zhuang,<sup>1,7</sup> A. D. McGuire,<sup>2</sup> K. P. O'Neill,<sup>3</sup> J. W. Harden,<sup>4</sup> V. E. Romanovsky,<sup>5</sup> and J. Yarie<sup>6</sup>

Received 22 August 2001; revised 29 January 2002; accepted 2 February 2002; published 14 December 2002.

[1] In this study, the dynamics of soil thermal, hydrologic, and ecosystem processes were coupled to project how the carbon budgets of boreal forests will respond to changes in atmospheric CO<sub>2</sub>, climate, and fire disturbance. The ability of the model to simulate gross primary production and ecosystem respiration was verified for a mature black spruce ecosystem in Canada, the age-dependent pattern of the simulated vegetation carbon was verified with inventory data on aboveground growth of Alaskan black spruce forests, and the model was applied to a postfire chronosequence in interior Alaska. The comparison between the simulated soil temperature and field-based estimates during the growing season (May to September) of 1997 revealed that the model was able to accurately simulate monthly temperatures at 10 cm ( $R > 0.93$ ) for control and burned stands of the fire chronosequence. Similarly, the simulated and field-based estimates of soil respiration for control and burned stands were correlated ( $R = 0.84$  and  $0.74$  for control and burned stands, respectively). The simulated and observed decadal to century-scale dynamics of soil temperature and carbon dynamics, which are represented by mean monthly values of these variables during the growing season, were correlated among stands ( $R = 0.93$  and  $0.71$  for soil temperature at 20- and 10-cm depths,  $R = 0.95$  and  $0.91$  for soil respiration and soil carbon, respectively). Sensitivity analyses indicate that along with differences in fire and climate history a number of other factors influence the response of carbon dynamics to fire disturbance. These factors include nitrogen fixation, the growth of moss, changes in the depth of the organic layer, soil drainage, and fire severity. **INDEX TERMS:** 1615 Global Change: Biogeochemical processes (4805); 0315 Atmospheric Composition and Structure: Biosphere/atmosphere interactions; 0330 Atmospheric Composition and Structure: Geochemical cycles; **KEYWORDS:** carbon, fire, nitrogen, hydrology, permafrost

**Citation:** Zhuang, Q., A. D. McGuire, K. P. O'Neill, J. W. Harden, V. E. Romanovsky, and J. Yarie, Modeling soil thermal and carbon dynamics of a fire chronosequence in interior Alaska, *J. Geophys. Res.*, 107, 8147, doi:10.1029/2001JD001244, 2002. [printed 108(D1), 2003]

### 1. Introduction

[2] High latitude ecosystems occupy a large proportion (22%) of the terrestrial surface and contain approximately 40% of the world's soil carbon inventory that is potentially responsive to near-term climate change [McGuire *et al.*, 1995; Melillo *et al.*, 1995; McGuire and Hobbie, 1997].

Among the world's biomes, boreal forests contain the largest soil carbon pools in the world [Post *et al.*, 1982; Gorham, 1991; Chapin and Mathews, 1993]. Much of the boreal forest is underlain by permafrost, which is susceptible to cycles of degradation (thermokarst) and aggradation [Thie, 1974]. These cycles have in some cases occurred in association with fire [Zoltai, 1993], which is a major disturbance in boreal forests [Kasischke *et al.*, 2000]. The thawing of permafrost after fire has the potential to change the thermal and moisture properties of the soil that have led to substantial soil carbon storage in boreal forest ecosystems.

[3] Fire disturbance in North America's boreal forests was higher in the 1980s than in any previous decade on record [Murphy *et al.*, 2000], and the area of western Canadian boreal forest burned annually has doubled in the last 20 years [Kasischke *et al.*, 2000]. Concurrently, annual surface temperatures in Alaskan boreal and arctic regions have increased 2° to 4°C during the last century [Lachenbruch and Marshall, 1986] and 1° to 2°C in recent decades [Osterkamp and Romanovsky, 1999]. The warming being experienced in Alaska during recent decades is part of a

<sup>1</sup>Department of Biology and Wildlife, University of Alaska Fairbanks, Fairbanks, Alaska, USA.

<sup>2</sup>U.S. Geological Survey, Alaska Cooperative Fish and Wildlife Research Unit, University of Alaska Fairbanks, Fairbanks, Alaska, USA.

<sup>3</sup>Forest Inventory & Analysis, North Central Research Station, USDA Forest Service, St. Paul, Minnesota, USA.

<sup>4</sup>U.S. Geological Survey ms 962, Menlo Park, California, USA.

<sup>5</sup>Geophysical Institute, University of Alaska Fairbanks, Fairbanks, Alaska, USA.

<sup>6</sup>Department of Forest Science, University of Alaska Fairbanks, Fairbanks, Alaska, USA.

<sup>7</sup>Now at The Ecosystems Center, Marine Biological Laboratory, Woods Hole, Massachusetts, USA.

warming trend that is occurring throughout northwestern North America [Beltrami and Mareschal, 1994; Oechel and Vourlitis, 1994; Serreze et al., 2000]. Permafrost throughout Alaska is also currently warming [Osterkamp and Romanovsky, 1999]. Some studies have indicated that wildfire activity may be related to the warming trend in North America. For example, fire regimes are sensitive to climate in both Alaska [Hess et al., 2001] and Canada [Stocks et al., 2000]. In addition, warming has been identified by Kurz et al. [1995] as a possible factor in the increasing fire frequency observed in Canada since 1970 [Kurz and Apps, 1995]. Analyses that have used simulations of changes in climate associated with doubled atmospheric CO<sub>2</sub> suggest that the boreal forest region could experience a 40% increase in the annual amount of area burned [Flannigan and Van Wagner, 1991]. Moreover, the prospect of summer drought, indicated by recent trends in Alaska [Wotton and Flannigan, 1993; Barber et al., 2000] threatens to increase the occurrence of fire.

[4] Changes in the fire regime of boreal forests may have consequences for the global carbon budget because fire disturbance substantially affects carbon storage of boreal forests by influencing both the structure and function of these ecosystems. Fire influences the structure of boreal forest ecosystems through influences on population and vegetation dynamics [Zackrisson, 1977; De Grandpre et al., 1993; Schimmel and Granstrom, 1996; Luc and Luc, 1998; Lynham, et al., 1998]. These structural changes have profound influences on the dynamics of permafrost, soil moisture, and soil nutrient cycles in boreal forests [Viereck, 1972, 1973; Dyrness et al., 1989; Wardle, et al., 1998; Driscoll, et al., 1999; Brais et al., 2000; Grogan, et al., 2000; Smith et al., 2000; Yoshikawa et al., 2002]. Some studies suggest that disturbance and growth patterns after disturbance at high latitudes may have contributed substantially to the approximately 15% increase in the amplitude of the seasonal cycle measured at some high latitude CO<sub>2</sub> monitoring stations since the 1960s [Randerson et al., 1997; Zimov et al., 1999]. Kurz and Apps [1999] also indicated that fire disturbance is one of the most important factors affecting the interaction of carbon and permafrost dynamics in North America. Furthermore, some studies have indicated that boreal forests may be a net source of CO<sub>2</sub> if warming greatly increases fire frequency or decomposition [Kasischke et al., 1995; Kurz and Apps, 1995].

[5] To evaluate the effects of fire disturbance on carbon source-sink activity in boreal forests, large-scale terrestrial biosphere models need to integrate the processes that influence the soil thermal, hydrological, and biogeochemical dynamics of boreal forest ecosystems. Fire disturbance interacts with all of these processes to influence soil carbon storage [Harden et al., 2000], moss recovery [Harden et al., 1998], and the timing of vegetation recovery [McMurtrie et al., 1995; Gower et al., 1996; Ryan et al., 1996; Waring and Running, 1998; Buchmann and Schulze, 1999; Schulze et al., 2000]. However, large-scale models have been slow to integrate interactions between fire disturbance and ecosystem dynamics because of the long timescales over which these disturbance effects persist and the lack of long-term studies to monitor these changes. In this study we take the important step of integrating interactions between fire disturbance and ecosystem dynamics of boreal forests in

interior Alaska into a large-scale ecosystem model, the STM-TEM [Zhuang et al., 2001].

## 2. Methods

### 2.1. Overview

[6] We modified the soil thermal model (STM) version of the Terrestrial Ecosystem Model (TEM), the STM-TEM [Zhuang et al., 2001], by updating the STM and the hydrological model (HM) to integrate more effectively soil thermal and hydrological dynamics. Modifications of the STM included simulating the effects of recovering moss and fibric organic matter on soil thermal dynamics after fire disturbance. The HM represents a major revision of the Water Balance Model (WBM) [Vorosmarty et al., 1989] of TEM, and was structured to simulate the hydrological dynamics of the STM soil profile by representing the soil profile as a three soil-layer system: (1) a moss plus fibric soil organic layer, (2) a humic organic soil layer, and (3) a mineral soil layer. Modifications to TEM included adding formulations to simulate the thickness of moss, canopy biomass, and leaf area index. The formulation for decomposition in TEM was also modified to consider soil moisture of the humic organic soil layer as calculated by the HM.

[7] The modified STM-TEM was parameterized for black spruce (*Picea mariana* (Mill.) B.S.P.) forests that have been studied at the Bonanza Creek Experimental Forest in interior Alaska as part of the Taiga Long Term Ecological Research (LTER) Program. We then verified the performance of the model by simulating (1) water fluxes, soil moisture, and carbon dynamics of black spruce stands that have been studied as part of the Boreal Ecosystem Atmosphere Study (BOREAS) in northern Manitoba, Canada (see Sellers et al. [1997] for general information on BOREAS), and (2) age-dependent patterns of aboveground vegetation carbon in interior Alaska. Next, we applied the model to a black spruce fire chronosequence in interior Alaska to evaluate its ability to simulate age-dependent patterns of soil thermal and carbon dynamics. Finally, we conducted sensitivity analyses for different scenarios of moss growth after fire, soil moisture conditions, and fire severity to gain insight into factors that might influence the large-scale application of the model.

### 2.2. Alaska Chronosequence

[8] A black spruce fire chronosequence was established in the eastern Tanana River Valley between the towns of Delta Junction and Tetlin Junction, Alaska [O'Neill, 2000; O'Neill et al., 2002]. Soil temperature, soil moisture, soil respiration, and soil carbon storage were measured in 1997 for both recently burned and older control stands of the chronosequence. The stands were disturbed by fire in 1996, 1994, 1990, 1987, 1915, and 1855. These stands are similar with respect to slope, drainage, soil texture, and ground vegetation. In this area, soils in mature black spruce stands typically remain frozen within a meter of the surface, and the upper portion of the soil profiles are composed of relatively undecomposed mosses, moss litter, and roots, or "fibric" organic layer (Agriculture Canada, 1987) that is approximately 25 cm thick in mature stands. This layer is comparable to "Moss plus Upper Duff" layers referred to by foresters and can be considered ground fuel for most boreal fires [Harden et al., 2000].

**Table 1.** Location, Site Characteristics, and History of Burning for Stands of the Fire Chronosequence in Interior Alaska

Year of Most Recent Burn	Stand Age (1997 as Base Year)	Year of Previous Burn	Location	Soil Series	Moss Thickness in 1997 (Feather Moss, Fiber, or Dead Moss), cm	Percentage of Ground Covered by Bryophytes	Depth of Organic Soil Layer, cm
1996	1	1825 (approx.)	Tetlin Jct.	Not classified	5.9 ± 1.6 <sup>a</sup>	No Measurement	19.8 ± 2.0 <sup>b</sup>
1994 (Severe)	3	1855 (approx.)	Hajdukovich	Volkmar silt loam	2.1 ± 2.9	65.1 ± 6.7	8.7 ± 4.2
1994 (Moderate)	3	1855 (approx.)	Hajdukovich	Volkmar silt loam	2.2 ± 1.9	65.1 ± 6.7	5.7 ± 3.5
1990	7	1915	Tok Jct.	Not classified	5.8 ± 2.3	27.0 ± 6.3	10.6 ± 3.0
1987	10	1825 (approx.)	Delta Jct.	Nenana silt loam	3.7 ± 3.2	39.4 ± 5.7	4.7 ± 2.1
1915	80	Unknown	Tok Jct.	Not classified	14.9 ± 6.6	66.8 ± 9.0	22.3 ± 4.1
1855	140	Unknown	Gerstle River	Saulich silt loam	23.1	72.5 ± 7.6	33.5

<sup>a</sup>Reported values represent the mean ± standard deviation of 20 measurements per plot.

<sup>b</sup>Organic soil layer does not include moss.

The lower part of the soil profile consists of highly decomposed and charred (humic) materials that have in many cases accumulated over decades to millennia [as per *Trumbore and Harden, 1997*] and are 20 to 35 cm thick in mature stands.

[9] Among the stands in the chronosequence, the moss plus fibric soil organic layer varied from 0 to 23 cm, the percentage of ground covered by bryophytes ranged from 0% to 73%, and the humic organic layer varied from 5 to 34 cm (Table 1). The mineral soil was characterized as silt loam or silty clay loam. The thickness of the organic horizons in these stands following fire, which was measured in 1997, varied as a function of fire severity. For example, the stand that burned in 1996 experienced a very light fire severity that left approximately 30 cm of uncombusted organic matter on the soil surface. In contrast, the stands that burned in 1990 and 1994 experienced a more moderate fire severity that resulted in approximately 10 cm of surface organic matter. Among the recently burned stands, the stand that burned in 1987 appears to have experienced the most severe fire with approximately 5 cm of surface organic matter remaining after the fire.

### 2.3. Model Development

[10] We modified the STM described by *Zhuang et al. [2001]* so the simulation of soil thermal dynamics depends on simulated variation of moss thickness, soil moisture, and snowpack instead of on prescribed values for these variables (see Figure 1a). The STM receives information on moss thickness from TEM and information on soil moisture and snowpack from the HM. We structured the HM to simulate the hydrological dynamics of the STM soil profile by representing the soil profile as a three soil-layer system (see Figure 1b): (1) a moss plus fibric soil organic layer, (2) a humic organic soil layer, and (3) a mineral soil layer. The HM also considers active layer depth as provided by the STM (Figure 1a) to simulate changes in soil moisture, runoff, and percolation of each of these soil layers (Figure 1b). To consider how canopy development influences hydrology after fire, we implemented Penman and Penman-Monteith formulations [*McNaughton, 1976; McNaughton and Jarvis, 1983*] to simulate evaporation and transpiration. This implementation requires leaf area index (LAI), which is provided by a formulation in TEM (see Figure 1a). See Appendix A for details of the formulations for simulating water fluxes in the HM.

[11] The TEM was designed to simulate how interactions among carbon and nitrogen dynamics influence carbon dynamics of terrestrial ecosystems at continental to global scales [see *McGuire et al., 2001*], and has been applied to high latitude regions in a number of studies [*Clein et al., 2000; 2002; McGuire et al., 2000a, 2000b; Amthor et al., 2001; Potter et al., 2001; Zhuang et al., 2001*]. Our modifications to TEM in this study were focused on integrating more effectively the simulation of biogeochemistry after fire with the soil thermal dynamics simulated by STM and the hydrology simulated by HM. After fire, the STM and HM require information from TEM on how the thickness of moss and leaf area index change (Figure 1a). Therefore, we modified TEM by including formulations to simulate changes in the thickness of moss, canopy biomass, and leaf area index as the stand recovers from disturbance. The TEM requires information from STM on soil temperature and from HM on soil moisture of the humic organic layer and on estimated actual evapotranspiration (EET) (Figure 1a). We modified TEM so that soil temperature and soil moisture of the humic organic soil layer influences the simulation of heterotrophic respiration, nitrogen mineralization, and nitrogen uptake by the vegetation. Similar to previous versions of TEM, EET influences the simulation of gross primary production (GPP).

[12] The formulation that we added to TEM for simulating the thickness of moss after fire disturbance is empirical and depends on the number of years after fire:

$$D_{moss} = a \times \left(1 - e^{(-b \times t)}\right) \quad (1)$$

where  $D_{moss}$  is moss thickness (cm),  $t$  is the number of years since fire, and  $a$  and  $b$  are empirically determined parameters. The fit of the model to measurements of moss thickness in stands of the fire chronosequence is highly significant ( $R = 0.97$ ,  $P < 0.01$ ,  $N = 6$ ) where  $a$  is 93.15 and  $b$  is 0.002 [*O'Neill, 2000*]. We caution the use of this empirical relationship as we feel that it is only appropriate for stands less than 200 years old in interior Alaska as the relationship does not reach equilibrium for stand ages of approximately 2000 years and does not accurately predict the relationship between moss thickness and age of black spruce stands studied in BOREAS [*Harden et al., 1997*].

[13] The function,  $f(\text{FOLIAGE})$ , which was first implemented in the version of TEM used by *McGuire et al.*



**Table 2.** Values and Sources of Parameters for the Hydrologic Model Used in This Study

Parameter	Definition	Value	Source and Comments
$C_p$	Specific heat of air, $J\ kg^{-1}\ ^\circ C^{-1}$	1010.0	See <i>Running and Coughlan</i> [1988]
$\rho_a$	Density of air, $kg\ m^{-3}$	1.292	See <i>Monteith</i> [1973]
$R_a$	Canopy aerodynamic resistance, $s\ m^{-1}$	5	See <i>Landsberg</i> [1986] and <i>Jarvis</i> [1976]
$G_{MAX}$	Maximum canopy conductance, $m\ s^{-1}$	0.0016	See <i>Running and Coughlan</i> [1988]
$\gamma$	Psychrometric constant, $mbar\ ^\circ C^{-1}$	0.662	See <i>Monteith and Unsworth</i> [1990]
$\lambda_w$	Latent heat of vaporization of water, $KJ\ kg^{-1}$	2442	The value for $25^\circ C$ , see <i>Monteith and Unsworth</i> [1990]
$E_R$	Dimensionless extinction coefficient of radiation through the canopy	0.5	Values range from 0.3 to 1.5, see <i>Landsberg</i> [1986]
$LWP_{MIN}$	Minimum leaf water potential inducing stomatal closure, MPa	0.5	See <i>Running and Coughlan</i> [1988]
$I_{RMAX}$	The maximum daily canopy interception of rain, $mm\ mm^{-1}$	0.26	Based on the work by <i>Helvey</i> [1971] and <i>Helvey and Patric</i> [1965]
$K$	Latent heat fusion, $MJ\ mm^{-1}\ M^{-2}$	$3.5 \times 10^5$	See <i>Coughlan</i> [1991]
$I_{SMAX}$	Snow interception rate, $mm\ LAI^{-1}\ d^{-1}$	0.5	See <i>Coughlan and Running</i> [1997]
$G_b$	The soil surface boundary layer Conductance, $mm\ s^{-1}$	10	Assumed as same as the value of 0.05 m tall vegetation, see <i>Grace</i> [1981]
$G_v$	The gas constant for water vapor, $m^{-3}\ kPa\ kg^{-1}\ K^{-1}$	0.462	See <i>Monteith</i> [1973]
$\mu$	Parameter for determining probable rain days	0.0017	From E. B. Rastetter (unpublished data, 1989)
$\alpha$	Snow albedo, $KJ\ kg^{-1}$	0.80	See <i>Aguado</i> [1985] and <i>Running and Coughlan</i> [1988]
$L_s$	Latent heat of sublimation, $KJ\ kg^{-1}$	2845.0	See <i>Coughlan</i> [1991]
$S_a$	Radiation absorptivity of snow, $KJ\ kg^{-1}$	0.6	See <i>Coughlan</i> [1991]
$PFC_{MO}$	Field capacity of moss plus fibric, %	51.6	Estimated
$PWP_{MO}$	Field wilting point of moss plus fibric layer, %	32.1	Estimated
$PF_A$	Coefficient A for relationship describing dependence of field capacity on mineral soil texture	24.75	See <i>McGuire et al.</i> [1995, 1997] and <i>Tian et al.</i> [1999]
$PF_B$	Coefficient B for relationship describing dependence of field capacity on mineral soil texture	16.025	See <i>McGuire et al.</i> [1995, 1997] and <i>Tian et al.</i> [1999]
$PW_A$	Coefficient A for relationship describing dependence of wilting point on mineral soil texture	24.75	See <i>McGuire et al.</i> [1995, 1997] and <i>Tian et al.</i> [1999]
$PW_B$	Coefficient B of relationship describing dependence of wilting point on mineral soil texture	3.025	See <i>McGuire et al.</i> [1995, 1997] and <i>Tian et al.</i> [1999]
$PCT_{slt}$	Percentage of silt in mineral soil, %	30.0	See <i>McGuire et al.</i> [1995, 1997] and <i>Tian et al.</i> [1999]
$PCT_{cly}$	Percentage of clay in mineral soil, %	45.0	See <i>McGuire et al.</i> [1995, 1997] and <i>Tian et al.</i> [1999]
$SOIL_{CAP}$	Soil water capacity, $m^3$	2350.0	See <i>Running and Coughlan</i> [1988]
$P_C$	Percolation coefficients for three layers	5.0 (Moss plus fibric) 4.5 (Humic organic layer) 4.0 (Mineral soil layer)	See <i>Neilson</i> [1993, 1995] and <i>Haxeltine</i> [1996]
$MO_{PO}$	Porosity of moss plus fibric layer, %	80.0	Estimated
$PCT_{POA}$	Coefficient A of relationship describing dependence of porosity on mineral soil texture	28.0	See <i>McGuire et al.</i> [1995, 1997] and <i>Tian et al.</i> [1999]
$PCT_{POB}$	Coefficient B of relationship describing dependence of porosity on mineral soil texture	33.0	See <i>McGuire et al.</i> [1995, 1997] and <i>Tian et al.</i> [1999]

where  $m_1$  and  $m_2$  are parameters, and  $f(C_V)$  is a hyperbolic function of the state variable for vegetation carbon ( $C_V$ ):

$$f(C_V) = \frac{m_3 \times C_V}{1.0 + m_4 \times C_V} \quad (4)$$

where  $m_3$  and  $m_4$  are parameters.

[14] The HM uses the monthly LAI calculated by TEM to simulate canopy transpiration. The calculation of monthly LAI by TEM depends on the parameter for specific leaf area (SLA) and on monthly canopy leaf biomass ( $C_{VL}$ ):

$$LAI = SLA \times C_{VL} \quad (5)$$

**Figure 1.** (opposite) (a) Overview of the model used in this study, which required coupling a hydrological model (HM) with a soil thermal model (STM) and a terrestrial ecosystem model (TEM). The HM receives information on active layer depth from the STM and information on leaf area index from TEM. The STM receives information on moss thickness from TEM and information on soil moisture and snowpack from the HM. The TEM receives information on soil temperature from STM and information on soil moisture and evapotranspiration from HM. (b) The HM considers the dynamics of eight state variables for water including (1) rain intercepted by the canopy ( $R_I$ ), (2) snow intercepted by the canopy ( $S_I$ ), (3) snow layer on the ground ( $G_S$ ), (4) moisture content of the moss plus fibric organic layer ( $M_{MO}$ ), (5) rainfall detention storage ( $R_{DS}$ ), (6) snowfall detention storage ( $S_{DS}$ ), (7) moisture content of the humic organic layer ( $M_{HU}$ ), and (8) moisture content of the mineral soil layer ( $M_{MI}$ ). The HM simulates changes in these state variables at monthly temporal resolution from the fluxes of water identified in Figure 2b, which include (1) Rainfall ( $R_F$ ), (2) Snowfall ( $S_F$ ), (3) canopy transpiration ( $T_C = T_{C1} + T_{C2}$ ), (4) canopy evaporation ( $E_C$ ), (5) throughfall of rain ( $R_{TH}$ ), (6) canopy snow sublimation ( $S_S$ ), (7) throughfall of snow ( $S_{TH}$ ), (8) ground snow sublimation ( $G_S$ ), (9) soil surface evaporation ( $E_M$ ), (10) snowmelt ( $S_M$ ), (11) percolation from moss plus fibric organic layer to humic organic layer ( $P_1$ ), (12) percolation from humic organic layer to mineral soil layer ( $P_2$ ), (13) runoff from the moss plus fibric layer to the rainfall detention storage pool ( $ROR_{MO}$ ), (14) runoff from the moss plus fibric layer to the snowmelt detention storage pool ( $ROS_{MO}$ ), (15) runoff from the rainfall detention storage pool to surface water networks ( $ROR_{DS}$ ), (16) runoff from the snowmelt detention storage pool to surface water networks ( $ROS_{DS}$ ), and (17) drainage from mineral soil layer to groundwater ( $D_R$ ).

**Table 3.** Values and Sources for Estimated Pools and Fluxes Used to Parameterize the Model for a Black Spruce Forest at Bonanza Creek, Alaska

Variable	Value <sup>a</sup>	Source and Comments
C <sub>V</sub>	3250	Based on the work of <i>Van Cleve et al.</i> [1983, Table 2], <i>Oechel and Van Cleve</i> [1986], <i>Gower et al.</i> [1997], and <i>Ryan et al.</i> [1997]
N <sub>V</sub>	15	Based on Table 2 by <i>Van Cleve et al.</i> [1983]
C <sub>S</sub>	15000	Based on the work of <i>O'Neill</i> [2000] and <i>O'Neill et al.</i> [2002]
N <sub>S</sub>	500	Based on Tables 10 and 13 in the work of <i>Van Cleve et al.</i> [1983]
N <sub>AV</sub>	0.5	Based on the work of <i>Weber and Van Cleve</i> [1984]
GPP	810	Based on procedures described by <i>Clein et al.</i> [2002]
NPP	150	Based on Table 3 by <i>Van Cleve et al.</i> [1983]
NPPSAT	230	Assume a maximum NPP increase of 50% to nitrogen fertilization
NUPTAKE	1.8	Based on the work of <i>Oechel and Van Cleve</i> [1986] and their application of recycling estimates from <i>Van Cleve et al.</i> [1983, Tables 3 and 7]

<sup>a</sup>Units for annual gross primary production (GPP), net primary production (NPP), and NPPSAT are g C m<sup>-2</sup> yr<sup>-1</sup>. Units for annual N uptake by vegetation are g N m<sup>-2</sup> yr<sup>-1</sup>. Units for vegetation carbon (C<sub>V</sub>) and soil carbon (C<sub>S</sub>) are g C m<sup>-2</sup>. Units for vegetation nitrogen (N<sub>V</sub>), soil N (N<sub>S</sub>), and inorganic N (N<sub>AV</sub>) are g N m<sup>-2</sup>.

in which monthly C<sub>VL</sub> is estimated as f(FOLIAGE) × C<sub>VLmax</sub> × f(PHENOLOGY). The function f(FOLIAGE) has also been incorporated into the formulation for nitrogen uptake in a fashion similar to its effect on GPP to represent the growth of fine root biomass after fire with the assumption that fine root biomass is correlated with canopy biomass.

[15] The flux R<sub>H</sub> represents decomposition of all soil organic matter in an ecosystem and is calculated at a monthly time step as follows:

$$R_H = K_d C_S f(M_V) e^{0.069H_T} \quad (6)$$

where K<sub>d</sub> is a rate-limiting parameter that defines the rate of decomposition at 0°C, C<sub>S</sub> is the quantity for the state variable that describes carbon in soil organic matter, M<sub>V</sub> is mean monthly volumetric soil moisture, and H<sub>T</sub> is mean monthly temperature of the humic organic soil layer simulated by the STM; note that H<sub>T</sub> can be less than 0°C. The M<sub>V</sub> is determined by the simulation of soil moisture for the humic organic soil layer by HM and STM (see Appendix A for details). The function f(M<sub>V</sub>), which is fully described by *Tian et al.* [1999], is a nonlinear relationship that models the effects of desiccation on microbial activity at low M<sub>V</sub> and the influence of oxygen availability on microbial activity at high M<sub>V</sub>, with an optimum at an intermediate level of M<sub>V</sub>. The fluxes for nitrogen uptake by the vegetation and net nitrogen mineralization have been modified so that they depend on the monthly temperature of humic soil layer simulated by STM and soil moisture of the humic organic soil layer simulated by HM.

#### 2.4. Model Parameterization and Verification

[16] The parameters of STM were based on the existing parameters for the black spruce forest ecosystems in Bonanza Creek Experimental Forest [*Zhuang et al.*, 2001]. However, the water content of each soil layer, which was defined as a parameter in the first version of STM, was

simulated dynamically by HM. Similarly, the thickness of the moss plus fibric organic layer, which was defined by a parameter in the first version of STM, also varies dynamically. However, the thickness of the humic organic layer is still specified by a parameter in this version of the STM. For parameters of snow and soil thermal properties, see *Zhuang et al.* [2001]. The values and sources for parameters in the formulations of vegetation canopy transpiration, canopy evaporation, canopy sublimation, soil surface evaporation, and snow sublimation in the HM are documented in Table 2.

[17] We calibrated the rate-limiting parameters of TEM based primarily on studies by the Taiga LTER Program for black spruce forest ecosystems located at the Bonanza Creek Experimental Forest near Fairbanks in interior Alaska (see Table 3 for information on the fluxes and pools used to calibrate the model). The calibration was similar to the procedures described by *Clein et al.* [2002] [see also *Amthor et al.*, 2001; *Zhuang et al.*, 2001]. In the formulation for f(FOLIAGE), we determined the parameters m<sub>1</sub>, m<sub>2</sub>, m<sub>3</sub>, and m<sub>4</sub> by calibrating the model to the forest inventory data on aboveground vegetation biomass for interior Alaska [*Yarie and Billings*, 2002]. The values of m<sub>1</sub>, m<sub>2</sub>, m<sub>3</sub>, and m<sub>4</sub> that we used in our simulations were 15.206, -0.3197, 0.0401, and 0.0001, respectively.

[18] To verify the model with respect to carbon fluxes, we conducted the simulation with the parameterization in BNZ site of LTER in Alaska for the old black spruce (OBS) site of the Northern Study Area (NSA) of BOREAS [*Sellers et al.*, 1997]. The simulation was conducted from 1975 to 1997 with the assumption that there is no permafrost in the ecosystem. To drive the model, we used local climate data (air temperature and precipitation) from 1975 to 1997 that were obtained from the Thompson Airport, a Canadian AES station located 40 km east of the NSA-OBS site [see *Zhuang et al.*, 2001; *Clein et al.*, 2002]. We compared the simulated carbon fluxes to monthly carbon fluxes estimates from 1994 through 1997 based on eddy covariance data [*Goulden et al.*, 1998], as updated by A. Dunn et al. (personal communication, 2001) [see also *Clein et al.*, 2002]. The carbon fluxes include monthly GPP and monthly ecosystem respiration (RESP). Net ecosystem production (NEP), which represents the net change in carbon storage of an ecosystem, is calculated as the difference between GPP and RESP assuming negligible loss of organic matter by processes such as leaching. These comparisons indicated that the model was able to reproduce the monthly carbon dynamics at the NSA-OBS site (Figure 2). For GPP and RESP, R were larger than 0.97, slopes of a linear regression were not significant from 1.0, and the intercepts were less than 10.0 g C m<sup>-2</sup> month<sup>-1</sup>. For NEP, the R between simulated and field-based estimates was substantially lower (0.54), the slope (0.46) was substantially different from 1.0, although the intercept was close to 0 (1.86 g C m<sup>-2</sup> month<sup>-1</sup>). The contrast among the comparisons for GPP, RESP, and NEP is similar to results obtained in a comparison of fluxes simulated by nine models for the NSA-OBS site [*Amthor et al.*, 2001].

[19] To verify the model with respect to the simulation of water fluxes and soil moisture, we conducted the simulations for the NSA-OBS site and for old black spruce forest site at the Southern Study Area of BOREAS (SSA-OBS). For the NSA-OBS simulation, the model was driven as described in the previous paragraph. For the SSA-OBS

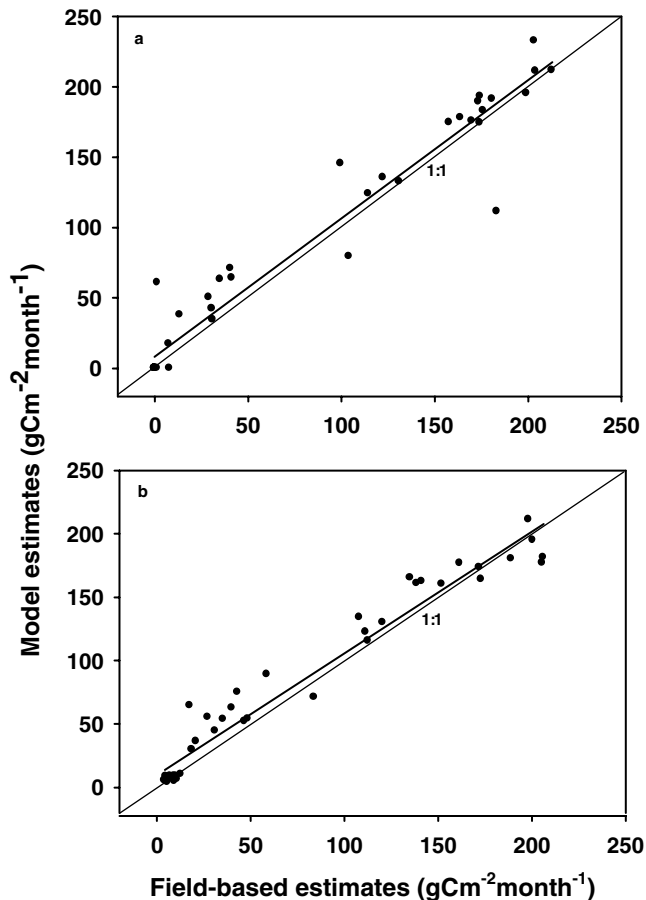


**Figure 2.** Comparison of monthly carbon fluxes between simulated and field-based estimates for an old black spruce forest in the northern study area of the boreal ecosystem atmosphere study (BOREAS). Linear regression between simulated and field-based estimates are compared with the 1:1 line. (a) Monthly estimates of gross primary production from 1994 to 1997; the linear regression was significant ( $P < 0.001$ ,  $N = 42$ ) with  $R = 0.97$ , slope = 0.98, and intercept =  $8.3 \text{ g C m}^{-2} \text{ month}^{-1}$ . (b) Monthly estimates of ecosystem respiration from 1994 to 1997; the linear regression was significant ( $P < 0.001$ ,  $N = 42$ ) with  $R = 0.98$ , slope = 0.96, and intercept =  $9.9 \text{ g C m}^{-2} \text{ month}^{-1}$ . Monthly field-based estimates were derived from eddy covariance data [Goulden *et al.*, 1998], as updated by Dunn *et al.* (personal communication) [see also Clein *et al.*, 2002].

simulation, we drove the model from 1975 through 1997 with climate data from Nipawin, which is a Canadian AES station not far from the SSA-OBS tower site. The simulation for SSA-OBS was conducted with the assumption that there is no permafrost in the ecosystem. Comparisons between simulated and field-based estimates indicated that the model reproduced seasonal patterns of evapotranspiration and soil moisture between 1994 and 1997 at both NSA-OBS and SSA-OBS (see Figure 3).

[20] To verify the age-dependent simulation of vegetation carbon, we ran the model to equilibrium, disturbed the stand with fire, and then drove the model for 178 years using mean monthly air temperature and precipitation that was derived by averaging monthly temperature and precipitation

data collected at Tok, Alaska between 1954 and 1999 [see <http://www.wrcc.dri.edu/summary/climsmak.html>]. Based on the work by Ryan [1991] and Ryan *et al.* [1997], we estimated aboveground vegetation carbon as 80% of total simulated vegetation carbon. For the inventory data, we estimated the aboveground vegetation carbon ( $\text{g C m}^{-2}$ ) by multiplying the inventory survey biomass data by 0.475 [see Atjay *et al.*, 1977]. The simulated and inventory-based aboveground vegetation carbon (Figure 4) were highly correlated ( $R = 0.95$ ,  $P < 0.001$ ,  $N = 12$ ), with a regression slope (0.95) that was not significantly different from 1.0, but an intercept ( $122.3 \text{ g C}$ ) that was significantly different from 0.0 ( $P < 0.001$ ,  $N = 12$ ).

## 2.5. Model Application to the Fire Chronosequence

[21] Before applying the model to the fire chronosequence we ran the model to equilibrium using an atmospheric  $\text{CO}_2$  level of 284 ppmv and the long-term mean monthly air temperature, precipitation, and cloudiness of the  $0.5^\circ$  grid cell with longitude  $143.0^\circ\text{W}$  and latitude  $63.5^\circ\text{N}$ , i.e., the Tok grid cell, from the long-term climate data set used in the simulations of McGuire *et al.* [2001]. For the equilibrium simulation, soil texture was extracted for the Tok grid cell from the data sets described by McGuire *et al.* [2001], and we set the initial soil thermal profile and its thermal properties to those of a mature black spruce forest at Bonanza Creek Experimental Forest that is underlain with permafrost similar to that described by Zhuang *et al.* [2001]. For the purposes of this study, we considered the results of the equilibrium solution to be representative of the year 1819. For the simulations over the period from 1820 through 1998, we drove the model with the atmospheric  $\text{CO}_2$  data set described by McGuire *et al.* [2001]. From 1820 through 1859 we drove the model with monthly temperature and precipitation corresponding the years 1860 through 1899 in the climate data from McGuire *et al.* [2001]. We used the monthly temperature and precipitation for the period from 1860 through 1953 of the Tok grid cell in the climate data from McGuire *et al.* [2001] to drive the model over those years. We used the climate data from the Tok weather station to drive the model from 1954 through 1998. From 1820 through 1998, we used the same monthly cloudiness data set that was used to drive the model to equilibrium in 1819.

[22] To apply the model to the fire chronosequence, we scheduled fires in 1825, 1855, and 1915 for the control stands, and in 1987, 1990, 1994, and 1996 for the recently burned stands (see Figure 5). The carbon and nitrogen pools of the recently burned stands were derived from the carbon and nitrogen pools of their respective control stands (see Figure 5). Thus, the pools of the stands that burned in 1990 and 1994 were derived from our simulations for the control stands that we estimate to have burned in 1915 and 1855, respectively (see Table 1 and Figure 5). Similarly, the pools of the stands that burned in 1987 and 1996 were derived from our simulation for the control stands that we estimate to have burned in approximately 1825 (Table 1 and Figure 5). We represent the control stands for the 1987 and 1996 burns with a single simulation; however, measurements were made in control stands that were unique to these burns. At the time of a scheduled disturbance, we assumed a constant severity for all fires in which 23% of vegetation carbon and nitrogen and 36% of soil organic carbon and

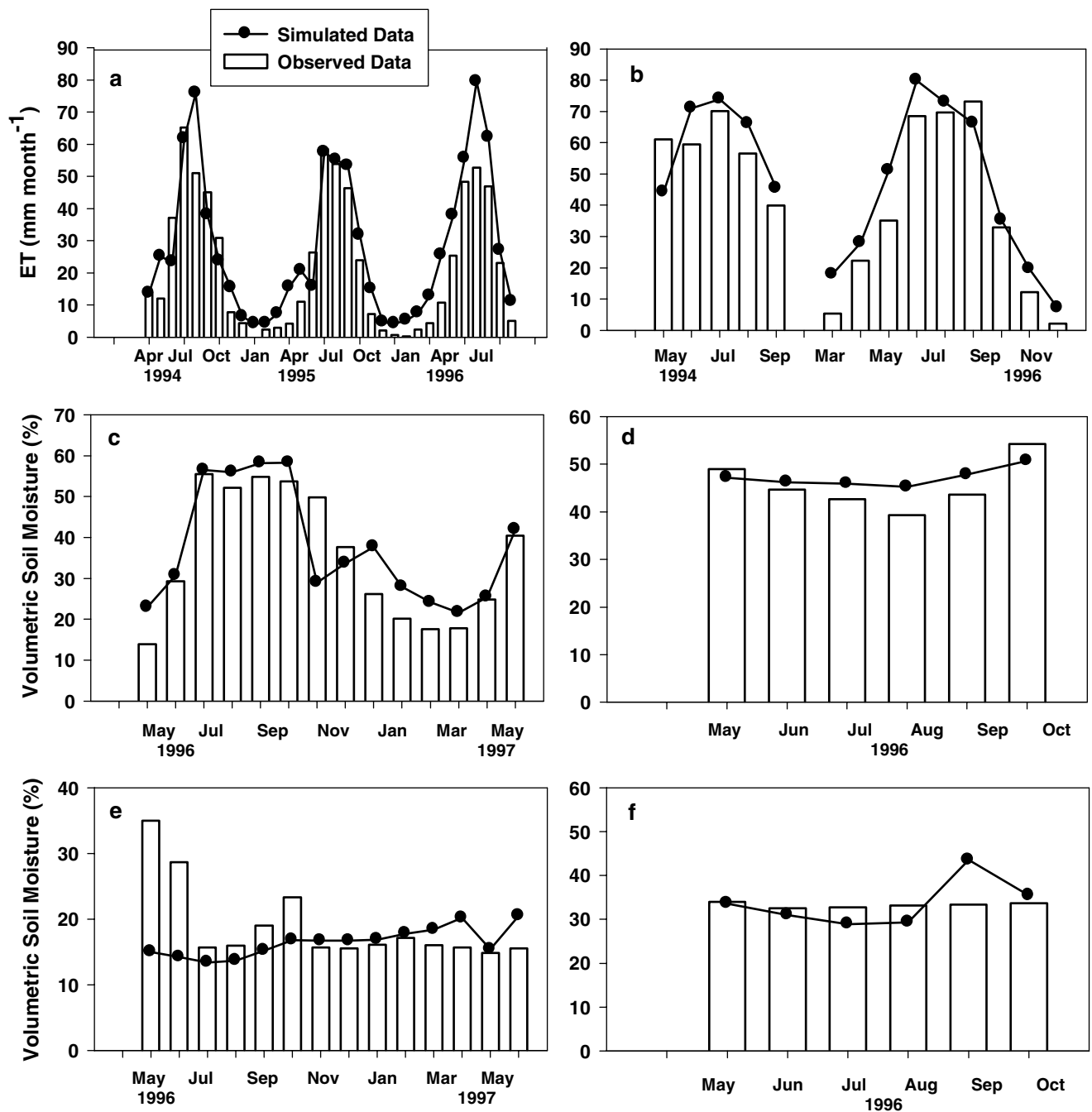


**Figure 3.** Comparison of monthly evapotranspiration and monthly volumetric soil moisture between simulated and field-based estimates for two old black spruce forests of the boreal ecosystem atmosphere study (BOREAS), one in the northern study area (NSA-OBS) and one in the southern study area (SSA-OBS). (a) and (b) Monthly estimates of evapotranspiration for NSA-OBS and SSA-OBS, respectively. (c) and (d) Monthly estimates of volumetric soil moisture of the humic organic soil layer for NSA-OBS and SSA-OBS, respectively. (e) and (f) Monthly estimates of volumetric soil moisture of the mineral soil layer for NSA-OBS and SSA-OBS, respectively. For comparison to simulations for NSA-OBS and SSA-OBS, we aggregated the tower-based estimates of evapotranspiration at half-hour resolution to monthly resolution. The half-hour resolution estimates of evapotranspiration were developed from eddy covariance measurements at the NSA-OBS site (*Goulden et al.* [1997, 1998], as updated by *Dunn et al.*, personal communication) and the SSA-OBS site [*Jarvis and Moncrieff*, 2000; *Newcomer et al.*, 2000]. Similarly, we aggregated daily or hourly measurements of volumetric soil moisture for the humic organic and mineral soil layers to monthly resolution for both the NSA-OBS and the SSA-OBS BOREAS sites. The humic organic soil moisture was estimated as the mean of all soil moisture measurements shallower than 45 cm, while the mineral soil moisture was estimated as the mean of all soil moisture measurements deeper than 45 cm and shallower than 105 cm.

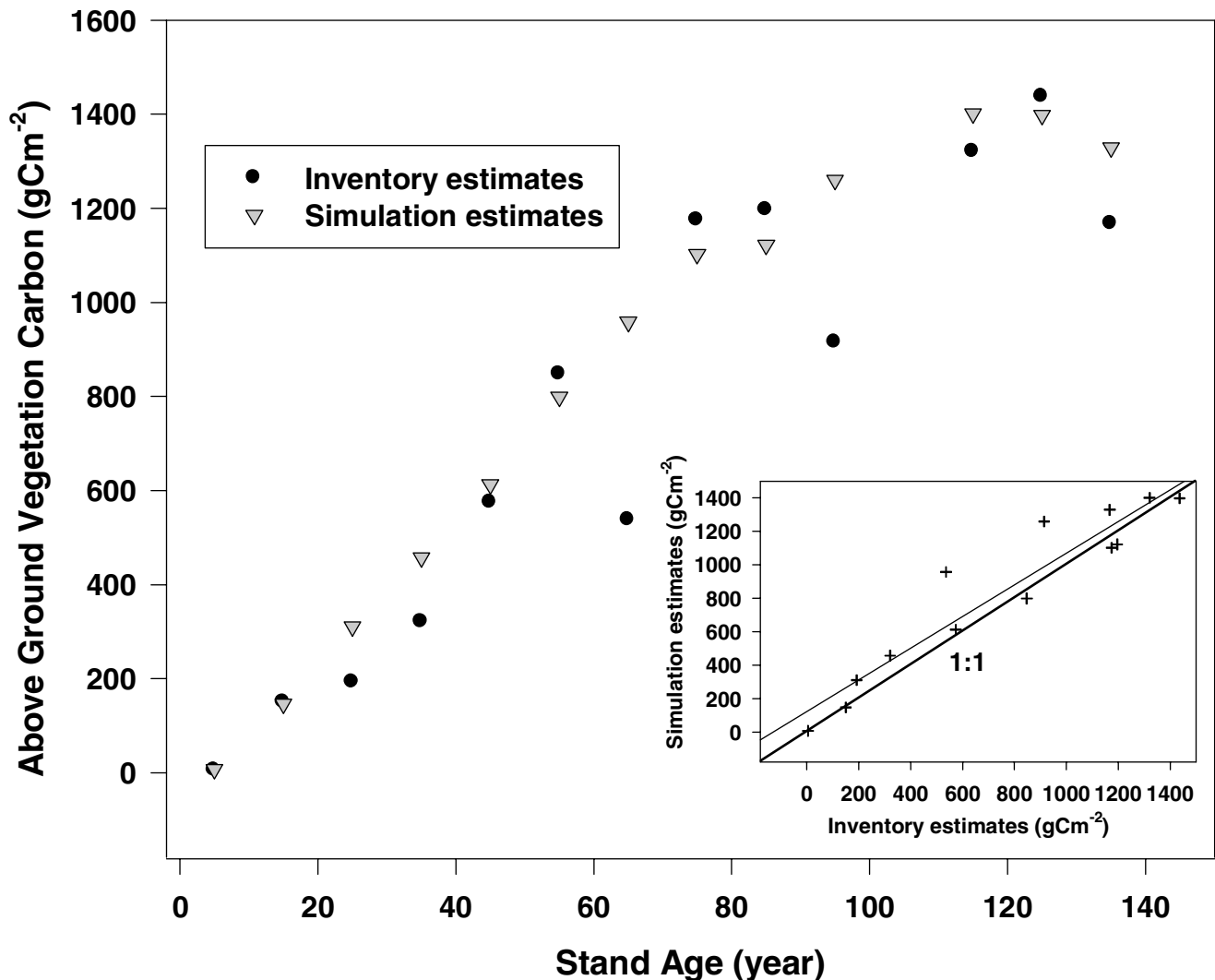


**Figure 4.** Comparison of simulated aboveground vegetation carbon with forest inventory estimates for black spruce forests in interior Alaska. The forest inventory estimates were derived from estimates of aboveground biomass in metric tons per hectare by *Yarie and Billings* [2002] for 10-year age intervals until age 100 and for 20-year age intervals between age 100 and 200. Linear regression between simulated and inventory-based estimates are compared with the 1:1 line in the inset.

nitrogen were consumed and released to the atmosphere in fire emissions. These values are typical of aboveground vegetation carbon and ground-layer carbon released from fire in interior Alaska [*French et al.*, 2000]. Of the vegetation carbon and nitrogen pools prior to disturbance, we assumed 1% is retained as live vegetation to start the growth of vegetation after fire. After accounting for vegetation carbon and nitrogen associated with fire emissions and with live vegetation remaining after fire, the remaining vegetation carbon and nitrogen from the pools prior to disturbance is added to the soil organic carbon and nitrogen pools. The simulations do not consider the fixation of nitrogen during the growth of vegetation after fire, although the nitrogen stocks of vegetation and soil have been adjusted in the initial equilibrium simulations so that target carbon to nitrogen ratios of vegetation and soil are maintained at equilibrium (see *McGuire et al.* [1997] for more details). In the simulations for the control sites that burned in 1855

and 1915, we prescribed the thickness of moss plus fibric organic layer and the humic organic layer by the site conditions in Table 1. In the simulation for the control sites that burned in 1825, we assumed that the soil profile was similar to the profile for the control site that burned in 1855. For the recently burned sites, we set the thickness of the moss plus fibric organic layer to 0 immediately after fire because more than 96% of the ground surface is either bare mineral soil or covered with char, and no live mosses are found [*O'Neill*, 2000]. We set the thickness of the humic organic layer in the recently burned sites to the value measured in 1997 (see Table 1).

[23] We compared soil temperatures at 10 cm and 20 cm depth, soil respiration, and soil carbon storage simulated for stands of the chronosequence to field-based estimates of these variables based on measurements made in 1997. Note that the field measurements of soil temperature at 10 cm and 20 cm will differ among the stands of the chronosequence as

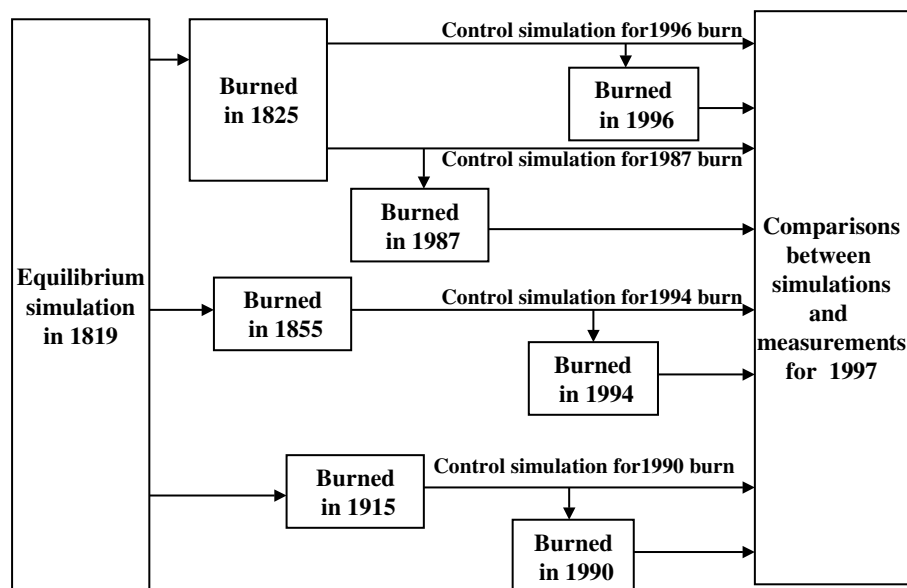


**Figure 5.** Flow diagram for the derivation of carbon and nitrogen pools in simulating ecosystem dynamics of the control and recently burned stands of the fire chronosequence in interior Alaska. All simulations start from equilibrium conditions in 1819. The control stands for the stands that recently burned in 1996 and 1987 are estimated to have last burned in approximately 1825. The control stands for the stands that recently burned in 1994 and 1990 are estimated to have burned in 1855 and 1915, respectively. Simulated estimates of soil temperature, soil respiration, and soil carbon in 1997 are compared to estimates based on field measurements made in 1997.

to whether the measurements are for fibric, humic, or mineral soil layers [O'Neill, 2000]. These differences do not affect our comparisons between simulated and field-based estimates as the thicknesses of moss and humic organic layers were similar between the simulations and the field conditions in 1997. For the burn that occurred in 1994, measurements were made in 1997 for two stands that experienced moderate and severe fires, respectively (see Table 1). Therefore, we averaged measurements for these two stands to develop field-based estimates of soil temperature, soil respiration, and soil carbon storage for the purpose of making comparisons to the simulation for the 1994 burn. We compared soil temperature and soil respiration at monthly resolution to evaluate seasonal dynamics and aggregated these variables over the growing season to evaluate long-term dynamics across the chronosequence. To estimate simulated soil respiration, we added  $R_H$  to an estimate of root respiration, which was calculated by multiplying simulated autotrophic respiration by 0.45 based on data for the ratio of root respiration to total autotrophic respiration for black spruce stands in BOREAS [Ryan *et al.*, 1997].

## 2.6. Sensitivity Analyses

[24] Sensitivity analyses were conducted for different scenarios of (1) moss growth, (2) soil moisture, and (3) fire severity. These analyses evaluated the responses of soil thermal, hydrological, nitrogen, and carbon dynamics to the different scenarios. For all simulations conducted for the sensitivity analyses, the model was run to equilibrium using a  $CO_2$  level of 284 ppmv, the monthly cloudiness data for the Tok grid cell from the cloudiness data set used in the model simulations of McGuire *et al.* [2001], and mean

monthly temperature and precipitation from the Tok weather station from 1954 to 1999 [see <http://www.wrcc.dri.edu/summary/climsmak.html>]. After reaching equilibrium, we initiated a fire and then ran the model for 140 years using the same input variables used to drive the model to equilibrium prior to fire disturbance.

[25] The sensitivity analysis to moss growth evaluated how documented moss growth after fire, i.e., the “standard” scenario, influences ecosystem dynamics relative to full moss cover in unburned stands and relative to a scenario in which moss does not grow after fire. In the standard scenario, moss cover is reduced to 0 immediately after fire, 23% of vegetation carbon and nitrogen are released to the atmosphere in fire emissions, 36% of soil carbon and nitrogen are released to the atmosphere in fire emissions, but the depth of the humic organic layer (30 cm) was not reduced by fire in this simulation. As soil drainage has the potential to influence soil moisture of the organic layer in permafrost soils, we were interested in evaluating how differences in soil moisture of the humic organic layer influences ecosystem dynamics. Therefore, we implemented two soil moisture scenarios in addition to the standard scenario in which volumetric soil moisture of the humic organic layer was prescribed to decrease or increase by 50% during both the equilibrium and postfire phases of the simulations.

[26] For the sensitivity analysis focused on fire severity, we implemented less severe and more severe scenarios relative to standard scenario, in which 23% of vegetation carbon and nitrogen and 36% of soil carbon and nitrogen were released to the atmosphere in fire emissions. In the less severe scenario, 12% of vegetation carbon and nitrogen and 18% of soil carbon and nitrogen are released as fire emissions. In the more severe scenario, 46% of vegetation

carbon and nitrogen and 54% of soil carbon and nitrogen are released as fire. In all scenarios, we assumed that the depth of moss plus fibric organic layer was 0 immediately after fire, and that the depth of the humic organic soil layer (30 cm) was reduced relative to the amount of soil carbon released (18% in the simulation with lower fire severity, 36% in the standard simulation, and 54% in the simulation with higher fire severity); however, the depth of this layer was not subsequently altered during the simulation of stand development after fire.

### 3. Results

#### 3.1. Soil Thermal Dynamics

[27] Comparisons between simulated and field-based estimates of soil temperature revealed that the model was able to accurately simulate monthly temperatures during the growing season for control and burned stands in the chronosequence (Figure 6). Most of the simulated monthly soil temperatures at 10 cm depth were within one standard deviation of the mean based on field measurements, and were significantly correlated to field-based estimates for both control stands (Figure 6a,  $R = 0.93$ ,  $P < 0.001$ ,  $N = 14$ ) and burned stands (Figure 6b,  $R = 0.93$ ,  $P < 0.001$ ,  $N = 14$ ). From May through September, simulated mean monthly temperature at 10 cm depth in burned stands was 2°C to 4°C warmer than in control stands. Across all months of the year, simulated mean monthly temperatures at 10 cm depth in burned sites were 3.3°C warmer than in control stands.

[28] Comparisons between simulated and field-based estimates of mean monthly growing season temperature (May–September) in the chronosequence revealed that the model was able to accurately simulate century scale dynamics of soil temperature after fire disturbance (Table 4). Across the chronosequence, the simulation of soil temperature at 20 cm depth ( $R = 0.93$ ,  $P < 0.01$ ,  $N = 6$ ) was more accurate than at 10 cm depth ( $R = 0.71$ ,  $P = 0.12$ ,  $N = 6$ ) because the simulation of soil temperature for the control stand that burned in 1855 was more accurate at 20 cm than at 10 cm (Table 4). With the exception of the 1996 burned site, the simulations indicated that younger stands generally had higher soil temperature than the older stands at both 10 cm and 20 cm depth. Starting with the 1994 site, the growing season soil temperatures decline with stand age from 11.8°C to 5.9°C at 10 cm and from 10.5°C to 3.6°C at 1855 burn site. Low temperatures observed in the 1996 burn site in both simulated and field-based estimates are likely associated with the low severity of fire at this stand, which left nearly 20 cm of humic organic material on the soil surface (Table 1). To evaluate this hypothesis, we conducted an additional simulation for the 1996 stand for a burn severity that had a depth of the humic organic layer equal to that of the 1994 stand that was severely burned. The simulation for a stand that was “severely burned” in 1996 resulted in warmer soil temperatures in comparison to the other stands. Thus, the thickness of the organic layer explains why soil temperature was colder than other stands that had burned less recently.

#### 3.2. Soil Respiration Dynamics

[29] Comparisons between simulated and field-based estimates of soil respiration revealed that the model was

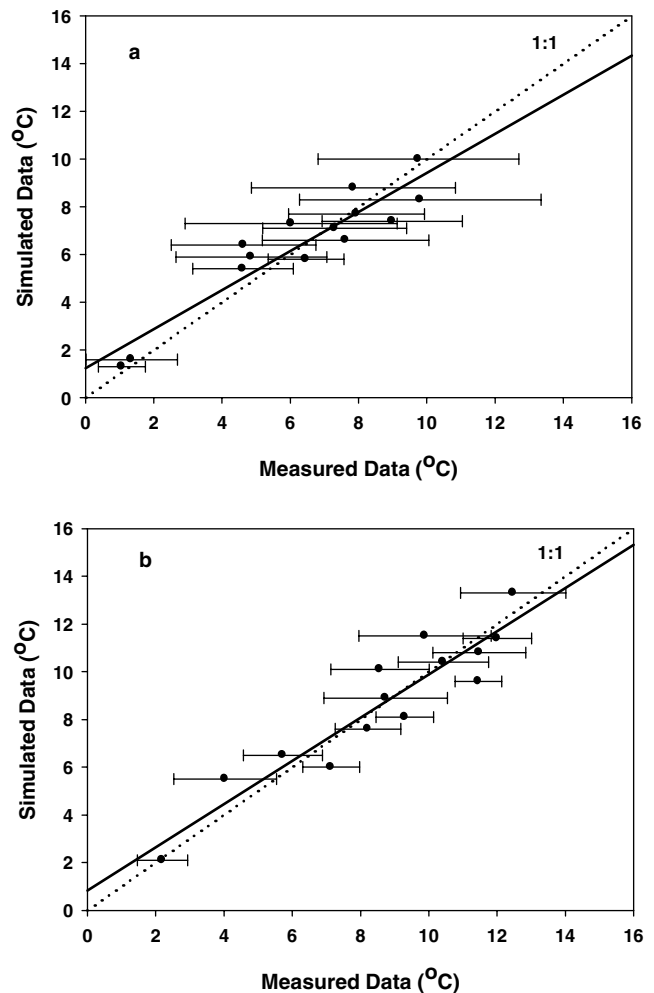


**Figure 6.** Comparison of regressions of monthly soil temperature estimates at 10 cm depth during the growing season in 1997 between simulated and field-based estimates with the 1:1 lines. The linear regressions were conducted using field-based estimates as the independent variable and simulated estimates as the dependent variable. (a) For control sites, the linear regression was significant ( $P < 0.001$ ,  $N = 14$ ) with  $R = 0.93$ , slope = 0.82, and intercept = 1.23°C. (b) For burned sites, the linear regression was significant ( $P < 0.001$ ,  $N = 14$ ) with  $R = 0.93$ , slope = 0.91, and intercept = 0.83°C. Field-based estimates (mean and standard deviation) were developed from data reported by O'Neill [2000] and O'Neill *et al.* [2002].

able to accurately simulate monthly soil respiration during the growing season for control and burned stands in the chronosequence (Figure 7). Most of the simulated estimates of monthly soil respiration were within one standard deviation of the mean based on field measurements (Figure 7), although the performance of the model for the control stands (Figure 7a;  $R = 0.84$ ,  $P < 0.01$ ,  $N = 17$ ) was generally better than burned stands (Figure 7b;  $R = 0.74$ ,  $P < 0.01$ ,  $N = 17$ ). Simulated soil respiration indicated that the burned sites had generally lower rates of soil respiration than control stands, particularly in recently burned sites; for example, fluxes simulated for the 1996 burned stand were

**Table 4.** Comparison Between Simulated and Field-Based Growing Season (May–September) Estimates in 1997 for Soil Temperature at 10 cm, Soil Temperature at 20 cm, Soil Respiration, and Soil Carbon for Stands of the Fire Chronosequence in Interior Alaska

Year of Most Burn	Soil temperature at 10 cm, <sup>a</sup> °C		Soil Temperature at 20 cm, <sup>a</sup> °C		Soil Respiration, <sup>b</sup> g C m <sup>-2</sup> month <sup>-1</sup>		Soil Carbon, <sup>c</sup> g C m <sup>-2</sup> yr <sup>-1</sup>	
	Field	Model	Field	Model	Field	Model	Field	Model
1996	6.8 ± 2.3	5.6	2.3 ± 1.9	4.3	60 ± 36	48	No measurement	10,120
1994	11.3 ± 2.4	11.8	9.7 ± 2.5	10.5	80 ± 41	78	8,920 ± 3,470	9,580
1990	10.0 ± 3.0	9.2	9.0 ± 2.5	8.1	92 ± 55	85	7,790 ± 3,640	9,160
1987	9.5 ± 2.6	9.1	7.4 ± 2.4	8.4	95 ± 45	85	8,230 ± 3,410	8,290
1915	5.6 ± 2.7	7.2	3.1 ± 1.8	5.0	108 ± 51	100	11,400 ± 2,010	11,950
1855	9.5 ± 3.2	5.9	4.0 ± 2.5	3.6	173 ± 75	160	15,770 ± 2,710	11,640

Values for field-based estimates represent monthly means ± standard deviation among sampling sites [see *O'Neill, 2000*; *O'Neill et al., 2002*] and values for simulated estimates represent monthly means.

<sup>a</sup>Soil temperature at 10 cm and 20 cm are relative to the surface of the soil.

<sup>b</sup>Soil respiration includes below-ground autotrophic respiration and decomposition.

<sup>c</sup>Field-based estimates represent the sum of carbon in the moss plus fibric and the humic organic layers. Standard deviation of field-based soil carbon estimates were based on the variance of differences equation by *Mosteller et al. [1961]*:  $\sigma_{\bar{x}-\bar{y}}^2 = \sigma_x^2 + \sigma_y^2$ .

approximately half those simulated for the control stand. Analysis of the simulated fluxes indicated that the reduction of soil respiration at the burned stand was primarily associated with the reduction of root respiration.

[30] Comparisons between simulated and field-based estimates of mean monthly growing season soil respiration (May–September) in the chronosequence revealed that the model was able to accurately simulate century scale dynamics of soil respiration after fire disturbance (Table 4;  $R = 0.95$ ,  $P < 0.01$ ;  $N = 6$  stands). Both simulated and field-based estimates of mean monthly soil respiration over the growing season increased with stand age. Analysis of the simulated fluxes indicated that increases in soil respiration with stand age were primarily associated with increases in root respiration.

### 3.3. Soil Carbon Dynamics

[31] In the year of fire disturbance, simulated soil carbon stocks of each of the stands in the chronosequence decrease (Figure 8a) because losses associated with the fire emissions are greater than gains associated with the input of dead vegetation carbon after the fire. For all stands in the chronosequence, the model simulates that the stand continues to lose soil carbon for a number of years while decomposition losses are greater than inputs of carbon to the soil from regrowing vegetation. In 1997, the model simulated that the recently burned stands (1996, 1994, 1990, and 1987) are losing soil carbon (Figure 8a). For the older stands that burned in 1825, 1855 and 1915, the model simulated that soil carbon is accumulating (Figure 8a) because carbon uptake by regrowing vegetation exceeds decomposition losses. Examination of the soil carbon trajectories indicates that it takes approximately 30 to 40 years after fire disturbance before soil carbon starts accumulating (Figure 8a). The simulations also indicate that the stand that burned in 1915 accumulated soil carbon at a faster rate than the stands that burned in 1825 and 1855. To evaluate factors responsible for the pattern, we conducted a set of simulations for the fire chronosequence using climate with no inter-annual variability and the same transient data set of atmospheric CO<sub>2</sub> that was used to drive the simulations represented in Figure 8a. The climate with no inter-annual variability was different than the equilibrium climate used to drive the simulations in Figure 8a, and resulted in different

equilibrium estimates of soil carbon (Figure 8b). The results of these new simulations (Figure 8b) suggest that along with differences in fire history, that the climate experienced by stands is an important factor responsible for the dynamics of soil carbon.

[32] For five of the stands in the chronosequence, soil carbon of each stand was estimated as the sum of carbon stored in moss, the fibric organic layer, and the humic organic layer from the 1997 measurements of *O'Neill et al. [2002]*; see also *O'Neill [2000]*. The simulated and field-based estimates of soil carbon among the five stands were highly correlated ( $R = 0.91$ ,  $P < 0.01$ ,  $N = 5$ ). The simulated estimates were most similar to field-based estimates of soil carbon for the four youngest stands, but the model underestimated soil carbon of the stand that burned in 1855 by about 30% (Table 4). While it is possible that the control stand that burned in 1855 may represent a biased site with respect to field-based estimates of soil carbon storage [*O'Neill, 2000*], additional simulations that we conducted with model suggest that nitrogen dynamics not represented in the model may play a role in the underestimate of soil carbon by the model for the control stand that burned in 1855 (Figures 8b and 8c). In the simulations that were driven by climate with no inter-annual variability, soil carbon stabilizes at approximately 11,000 g C m<sup>-2</sup> instead of the initial steady state value of between 15,000 and 16,000 g C m<sup>-2</sup> (Figure 8b). We hypothesized that the stabilization at approximately 11,000 g C m<sup>-2</sup>, and hence the underestimate for the stand that burned in 1855, was associated with the fact that nitrogen was not added to the stand after disturbance. To test this hypothesis, we conducted a set of simulations in which we added nitrogen in equal amounts each year (approximately 2.5 g N m<sup>-2</sup>) over the course of the simulation to replace the nitrogen lost in fire emissions. We drove these simulations with the same data sets of climate and atmospheric CO<sub>2</sub> concentration that were used to drive the simulations of Figure 8b. In the simulation for the stand that was burned in 1855, soil carbon was estimated to be approximately 16,000 g C m<sup>-2</sup> (Figure 8c), which is similar to the soil carbon measured for that stand (Table 4). In comparison to the simulations with no nitrogen inputs after disturbance, the higher level of soil carbon storage simulated with nitrogen inputs was associated with NPP that was sustained at a higher level after the

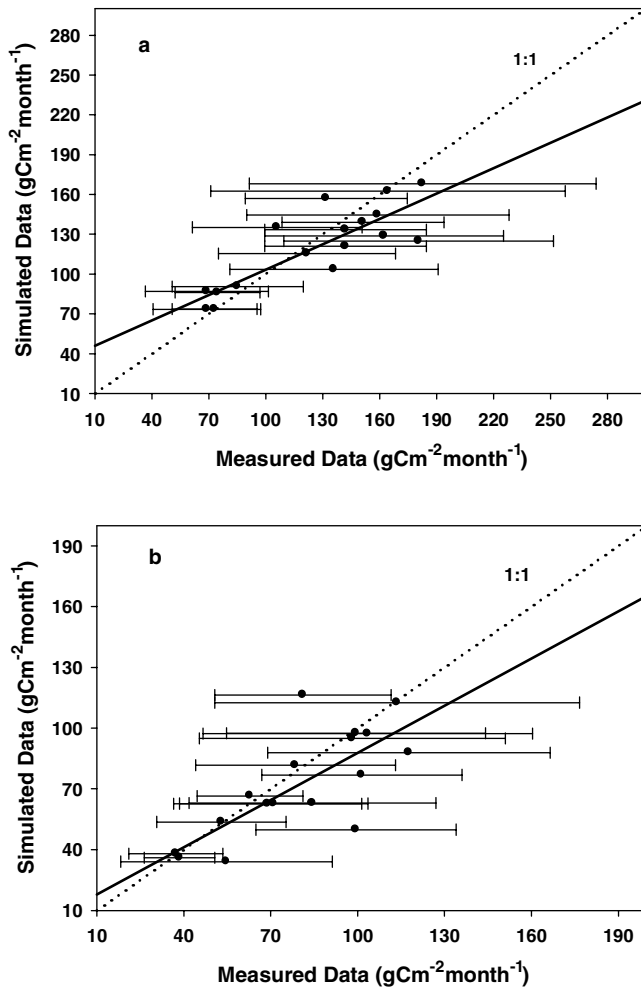


**Figure 7.** Comparison of regressions of monthly soil respiration estimates during the growing season in 1997 between simulated and field-based estimates with the 1:1 lines. The linear regressions were conducted using field-based estimates as the independent variable and simulated estimates as the dependent variable. (a) For control sites, the linear regression was significant ( $P < 0.001$ ,  $N = 17$ ) with  $R = 0.84$ , slope = 0.64, and intercept =  $39.6 \text{ g C m}^{-2} \text{ month}^{-1}$ . (b) For burned sites, the linear regression was significant ( $P < 0.001$ ,  $N = 17$ ) with  $R = 0.75$ , slope = 0.78, and intercept =  $10.2 \text{ g C m}^{-2} \text{ month}^{-1}$ . Field-based estimates (mean and standard deviation) were developed from data reported by O'Neill [2000] and O'Neill et al. [2002].

vegetation had substantially recovered from the fire. Thus, our simulations suggest that nitrogen fixation after fire is an important issue to consider in long-term responses of soil carbon after fire disturbance.

### 3.4. Sensitivity Analyses

#### 3.4.1. Sensitivity to Moss Growth

[33] The simulations indicated that moss growth clearly affects the long-term dynamics of soil temperature after fire, in which the burned stands are approximately  $4^\circ\text{C}$  warmer immediately after fire, and is responsible for a return toward colder soil temperatures of the unburned stand (Figure 9a).

[34] The development of the moss layer also influences the long-term dynamics of soil moisture after fire (Figure 9b), although this effect is less striking than the effect of moss on soil temperature. For approximately the first 50 years after fire, the mean volumetric soil moisture (VSM) from May to September for the simulations of the burned stands is much lower than the unburned stand because of two factors: (1) higher evaporation as more radiation reaches the soil surface associated with a reduced canopy, and (2) greater drainage associated with a thicker active layer after fire. Soil moisture starts to increase about 50 years after fire in these simulations (Figure 9b) as the canopy closes, which causes soil surface evaporation to decrease, and as moss layer thickens, which causes drainage to be impeded as the active layer become thinner. After approximately 100 years, soil moisture in the stand with moss growth stabilizes at the same level as the unburned stand as moss growth, leaf area index, and active layer depth stabilize. The dynamics of soil moisture in the stand without moss growth slightly lags the dynamics of the stand with moss growth (Figure 9b) because the stand without moss growth has higher surface evaporation than the stand with moss growth for the same leaf area.

[35] The effect of moss growth on soil temperature influenced patterns of decomposition and net nitrogen mineralization during stand development. Decomposition gradually decreased after fire because of declines in soil carbon associated with lower inputs of carbon from the vegetation (Figure 9e), but gradually increased through stand development as inputs to soil carbon from vegetation increased along with increases in NPP (Figure 9d). Immediately after fire, our simulations indicated that net nitrogen mineralization drops substantially (Figure 9c) because of immobilization that is enhanced by the high levels of inorganic nitrogen that build up in association with much reduced levels of plant nitrogen uptake. Simulated nitrogen cycling rates gradually increase through stand development after fire (Figure 9c), with higher rates in the simulation with no moss growth after about 60 years that appear to be caused by higher rates of decomposition ( $R_H$ ; Figure 9e) that are associated with higher soil temperature.

[36] Differences in net nitrogen mineralization between the simulations with and without moss growth translated into differences in NPP (Figure 9d), with higher NPP in the simulation without moss growth. In comparison to the unburned stand, NPP stabilizes at a lower level in the burned stands because nitrogen lost in fire emissions was not replaced during stand development after fire. While the growth of moss influenced the simulated dynamics of both NPP and decomposition, it had no effect on the long-term dynamics of NEP (Figure 9f). However, the growth of moss does influence the allocation of carbon storage, as the simulation with moss growth has lower levels of vegetation carbon storage (Figure 9g) and slightly higher levels of soil carbon storage (Figure 9h).

#### 3.4.2. Sensitivity to Moisture Conditions

[37] In the standard scenario, which was the same as the scenario with moss growth after fire in the previous sensitivity analysis, mean VSM from May to September drops to less than 25% after fire disturbance and returns to approximately 35% after about 100 years of stand development (Figure 10a). In the low soil moisture scenario, May–

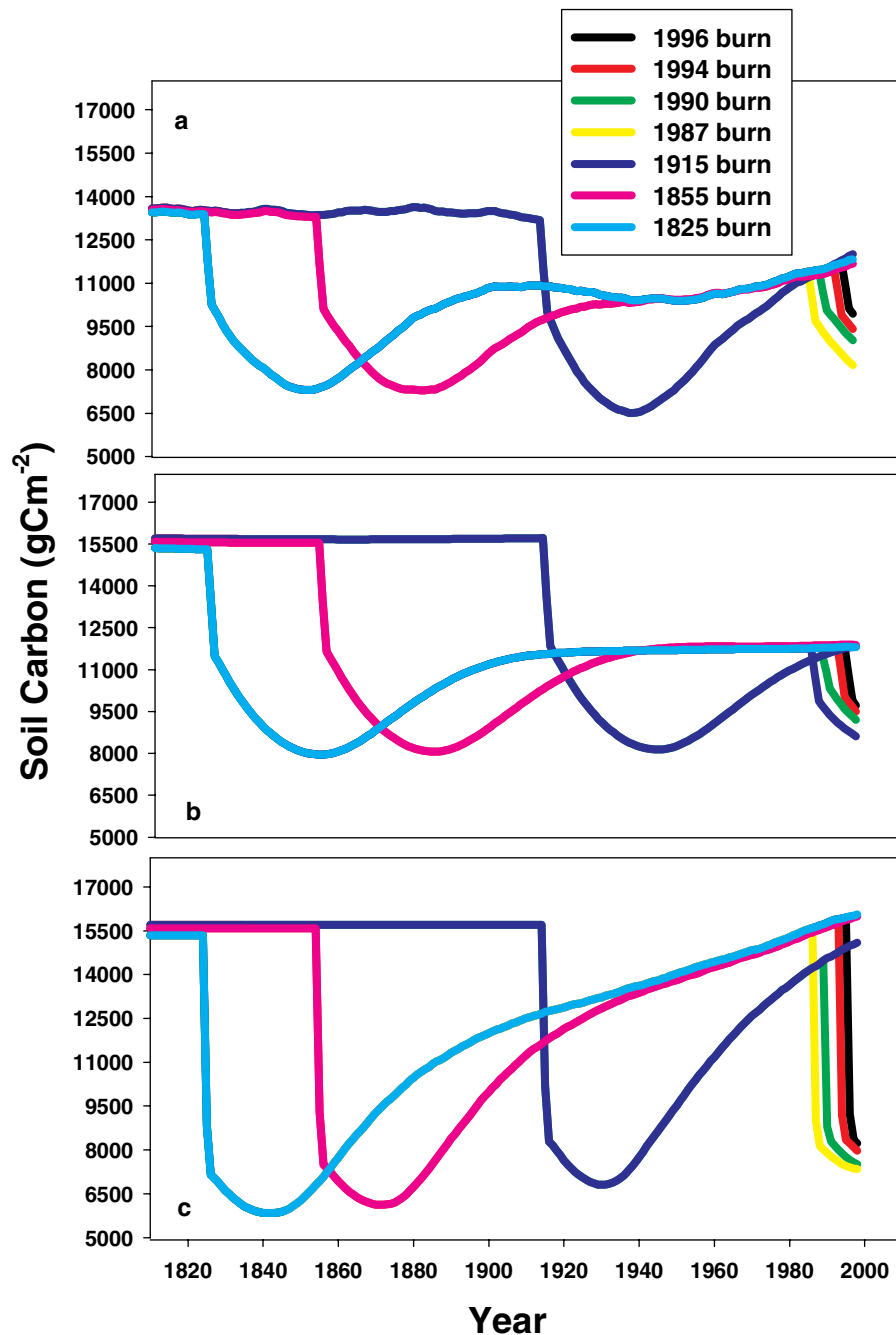


**Figure 8.** Simulated soil carbon dynamics for control stands (last burned in 1825, 1855, and 1915) and recently burned stands (burned in 1987, 1990, 1994, and 1996) of the fire chronosequence in interior Alaska. (a) Simulations driven with transient climate, transient atmospheric  $\text{CO}_2$ , and no nitrogen inputs. (b) Simulations driven with constant climate data, transient atmospheric  $\text{CO}_2$ , and no nitrogen inputs. (c) Simulations driven with constant climate, transient atmospheric  $\text{CO}_2$ , and the addition during stand development of nitrogen that was lost during fire.

September VSM drops to approximately 12% after fire and increases to about 18% through stand development, while the high moisture scenario May–September VSM drops to about 36% after stand development and increases to approximately 52% (Figure 10a). It is important to note that the 52% VSM level in the high moisture scenario is approximately the same as the 50% VSM optimum for the function  $f(M_V)$  in equation (6) for  $R_H$  [see Tian *et al.*, 1999], above

which anaerobic conditions start to retard decomposition in the model.

[38] Soil moisture conditions played an important role in controlling soil temperature and in regulating rates of decomposition and net nitrogen mineralization. The simulations indicate that lower levels of soil moisture lead to higher soil temperatures immediately after fire with approximately  $1^\circ\text{C}$  difference at 20 cm depth among scenarios

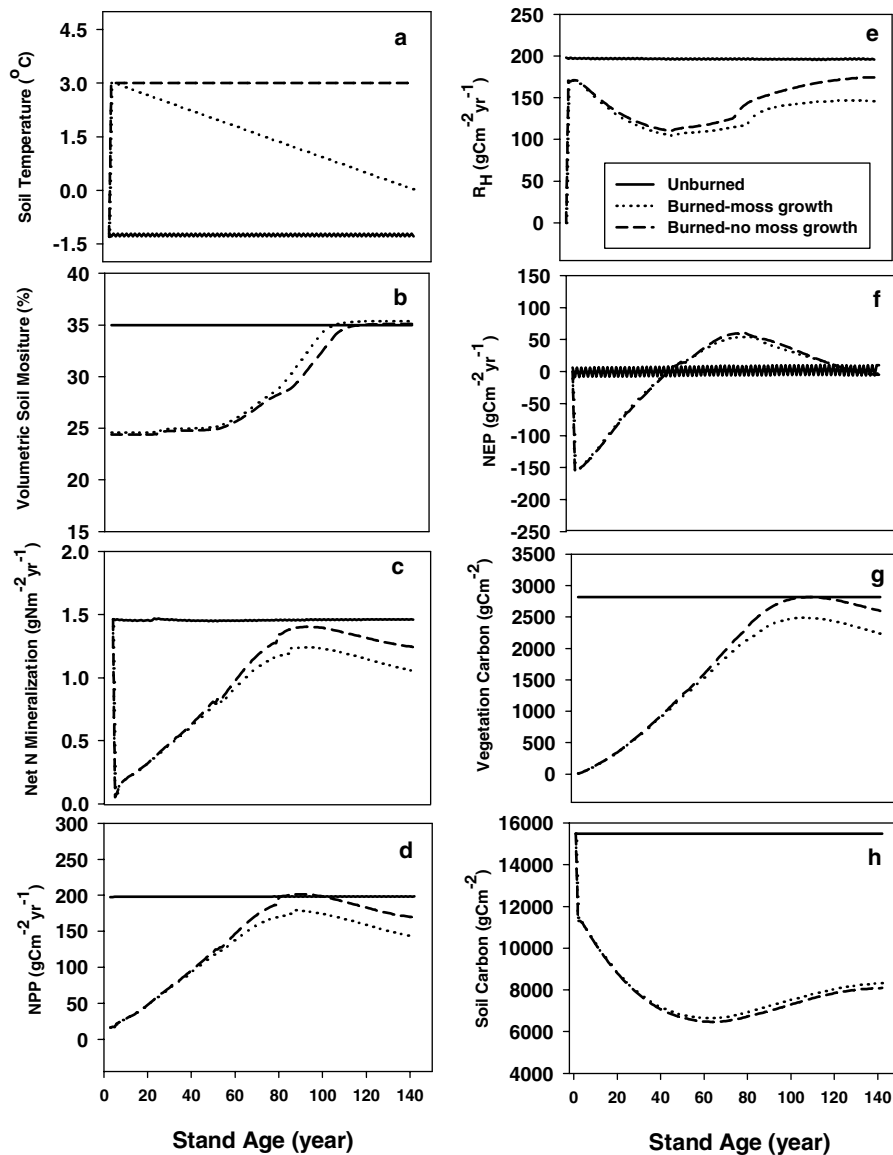


**Figure 9.** The dynamics of soil temperature, soil moisture, nitrogen cycling, carbon fluxes, and carbon stocks in the sensitivity analysis for moss growth. Scenarios include a stand with moss cover that was not burned (unburned), a stand that was burned and moss was allowed to grow during stand development (burned - moss growth; also known as the “standard” scenario), and a stand that was burned and moss was not allowed to grow during stand development (burned - no moss growth). (a) soil temperature integrated over 20 cm of soil relative to the soil surface, (b) mean volumetric soil moisture of the humic organic layer from May to September, (c) annual net nitrogen mineralization, (d) annual net primary production (NPP), (e) annual heterotrophic respiration/decomposition ( $R_H$ ), (f) annual net ecosystem production (NEP), (g) vegetation carbon, and (h) soil carbon.

(Figure 10b). Higher soil temperature is maintained throughout stand development for the duration of the simulations in the scenarios with lower soil moisture (Figure 10b). Differences in soil moisture among the scenarios explain differences in decomposition rates (Figure 10e) that were responsible for differences in rates of net nitrogen mineralization (Figure 10c). Thus, in contrast to the sensitivity analysis for moss growth in which differences in soil temperature drove differences in decomposition and net nitrogen mineralization, differences in soil moisture were more important than differences in soil temperature in the

responses of decomposition and net nitrogen mineralization in this sensitivity analysis to soil moisture.

[39] Differences in net nitrogen mineralization among the scenarios translated into differences in NPP (Figure 10d), with higher NPP in the simulations with higher soil moisture. While NPP of the standard scenario stabilizes at a lower level than NPP of the unburned stand of Figure 9d because nitrogen lost in fire emissions was not replaced during stand development after fire, differences in soil moisture lead to larger differences in NPP among the moisture scenarios (Figure 10d) with higher NPP in the

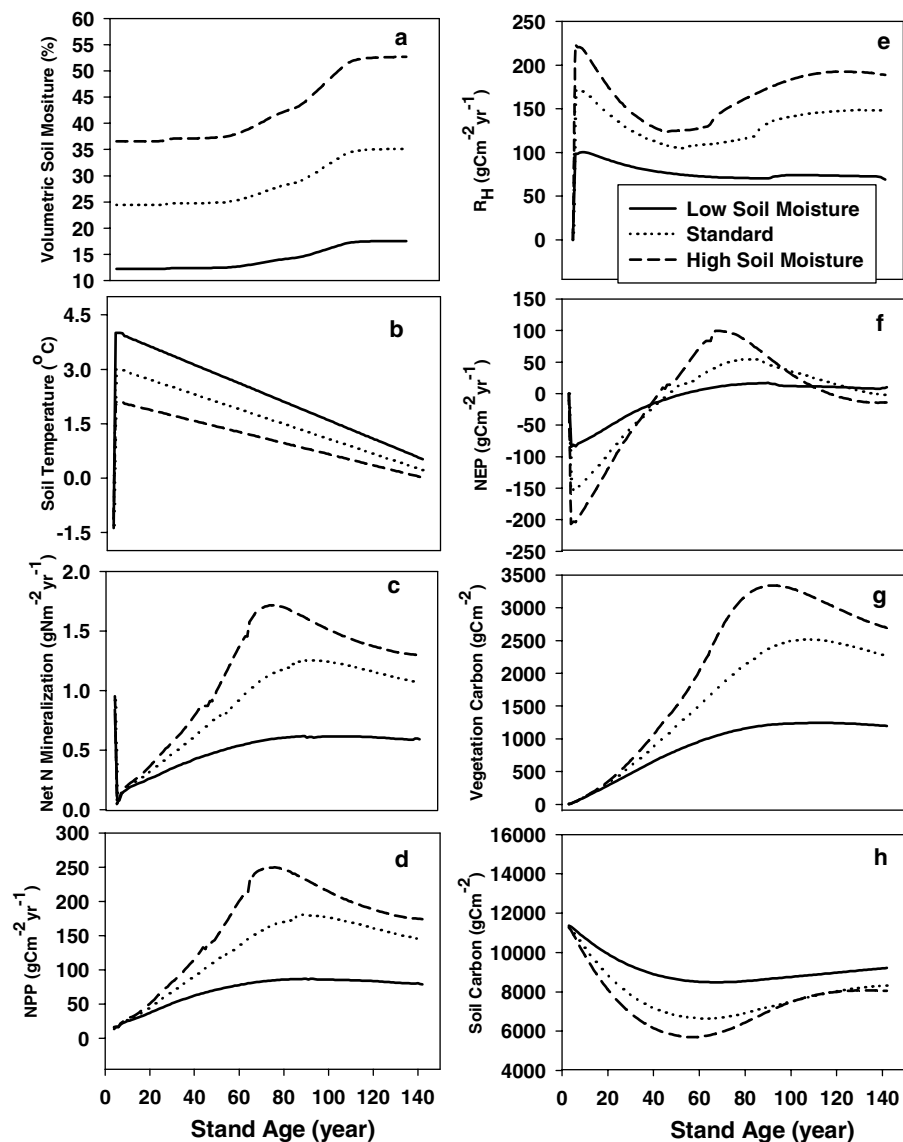


**Figure 10.** The dynamics of soil moisture, soil temperature, nitrogen cycling, carbon fluxes, and carbon stocks in the sensitivity analysis for soil moisture. Scenarios include the standard scenario, which is the same as the scenario for the burned stand with moss growth in Figure 9, and scenarios in which volumetric soil moisture of the standard scenario was prescribed to be 50% higher (high moisture) and 50% lower (low moisture). (a) mean volumetric soil moisture of the humic organic layer from May to September, (b) soil temperature integrated over 20 cm of soil relative to the soil surface, (c) annual net nitrogen mineralization, (d) annual net primary production (NPP), (e) annual heterotrophic respiration/decomposition ( $R_H$ ), (f) annual net ecosystem production (NEP), (g) vegetation carbon, and (h) soil carbon.

wetter soils because of higher nitrogen cycling rates (Figure 10c).

[40] For about 60 years after fire, the higher decomposition rates of the wetter scenarios caused lower NEP and higher postfire losses of carbon from the ecosystem over this period (Figure 10f). This response is relevant to soil moisture increases over the range of soil moisture for aerobic decomposition, and not over the range of soil moisture that leads to anaerobic conditions. In contrast, between approximately 60 and 140 years after fire, the higher NPP of the wetter scenarios caused higher NEP and higher rates of carbon accumulation in the ecosystem over

this period (Figure 10f). The different moisture scenarios influenced the allocation of carbon storage, as the wetter simulations led to more vegetation carbon accumulation and less soil carbon accumulation (Figures 10g and 10h).

### 3.4.3. Sensitivity to Fire Severity

[41] The simulations indicated that the effects of fire severity on the depth of the organic layer clearly affects the long-term dynamics of soil temperature after fire. Immediately after fire, a shallower humic organic layer associated with higher levels of fire severity lead to higher soil temperatures with approximately  $1.5^{\circ}\text{C}$  difference at 20 cm depth among scenarios (Figure 11a). Higher soil temper-

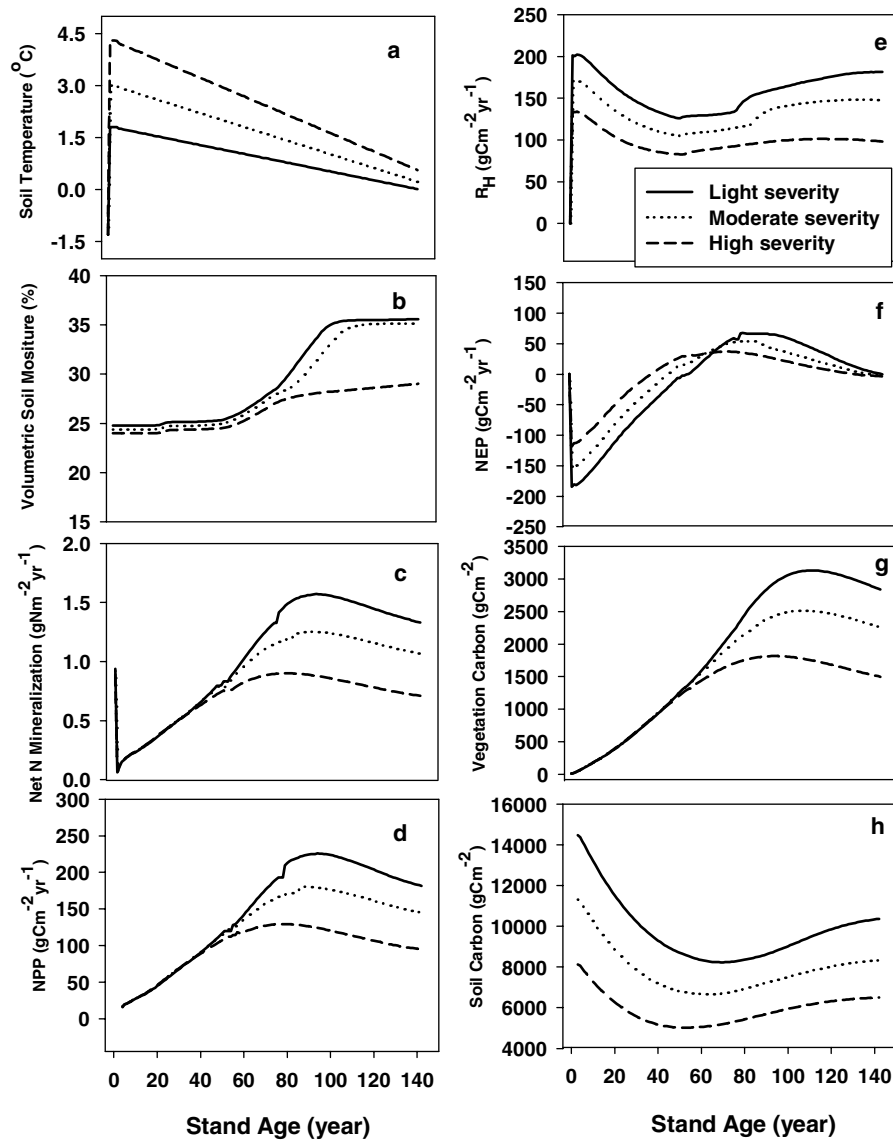


**Figure 11.** The dynamics of soil temperature, soil moisture, nitrogen cycling, carbon fluxes, and carbon stocks in the sensitivity analysis for fire severity. Scenarios include stands that experienced light burn severity (12% vegetation and 18% soil carbon and nitrogen released in fire emissions), moderate burn severity (23% vegetation and 36% soil carbon and nitrogen released in fire emissions), and severe burn severity (46% vegetation and 54% soil carbon and nitrogen released in fire emissions). The thickness of the organic layer was decreased by 18%, 36%, and 54% of 30 cm for the light burn, moderate burn, and severe burn scenarios, respectively. (a) soil temperature integrated over 20 cm of soil relative to the soil surface, (b) mean volumetric soil moisture of the humic organic layer from May to September, (c) annual net nitrogen mineralization, (d) annual net primary production (NPP), (e) annual heterotrophic respiration/decomposition ( $R_H$ ), (f) annual net ecosystem production (NEP), (g) vegetation carbon, and (h) soil carbon.

ature was maintained throughout stand development for the duration of the simulations in the scenarios with higher fire severity (Figure 11a).

[42] Among the scenarios, there was little effect of fire severity on soil moisture for about 60 years after fire (Figure 11b), after which May–September VSM increased as the canopy closed and eventually stabilized as leaf area stabilized. Although the soil moisture dynamics of the standard scenario slightly lagged the dynamics of the lightly burned scenario between approximately 60 and 110 years

after fire, the two scenarios stabilized at approximately the same level of soil moisture (Figure 11b). In contrast, the effects of fire severity on soil moisture dynamics were most pronounced for the severely burned stand (Figure 11b), which stabilized at soil moisture levels substantially lower than the other two scenarios because of greater drainage associated with a thicker active layer that results from higher soil temperatures.

[43] In contrast to the sensitivity analyses for moss growth and moisture conditions, in which effects of soil

temperature and soil moisture explained differences in decomposition among scenarios, higher decomposition rates occurred in the scenarios with lower fire severity (Figure 11e) because the labile pools of soil organic matter were higher in the scenarios with lower fire severity. This pattern occurred even though soil temperatures were higher in the simulations with higher fire severity. Higher decomposition rates in the scenarios with lower fire severity lead to higher rates of net nitrogen mineralization only after about 50 years of stand development (Figure 11c), as it appears that among the scenarios the effects of soil temperature and soil moisture on nitrogen immobilization rates compensated for effects of decomposition on gross nitrogen mineralization rates during the first 50 years after fire. As in the other sensitivity analyses, patterns of net nitrogen mineralization among the scenarios translated into patterns of NPP (Figure 11d). The decomposition, nitrogen mineralization, and NPP in the more severely burned scenarios do not recover to prefire levels because nitrogen lost in fire emissions was not replaced during stand development in these simulations.

[44] For about 60 years after fire, the higher decomposition rates of the scenarios with lower fire severity caused lower NEP and higher postfire losses of carbon from the ecosystem over this period (Figure 11f). In contrast, between approximately 60 and 140 years after fire, the higher NPP of the scenarios with lower fire severity caused higher NEP and higher rates of carbon accumulation in the ecosystem over this period (Figure 11f). The different scenarios of fire severity influenced the magnitude of carbon storage, as the scenarios with higher fire severity led to both less vegetation carbon accumulation and less soil carbon accumulation by the end of the simulation (Figures 11g and 11h). Lower carbon accumulation in the more severe fire scenarios occurs because of more nitrogen lost from the ecosystem in fire emissions.

## 4. Discussion

[45] Traditionally, the role of fire in carbon storage of forests in the boreal region has been estimated with book-keeping models [Kasischke et al., 1995; Kurz and Apps, 1999; Harden et al., 2000]. As fire disturbance is likely to interact with other factors in complex ways that affect carbon dynamics, it is important to synthesize understanding from field studies into process-based models that represent the mechanisms responsible for these interactions. We applied the STM-TEM in this study to a fire chronosequence in interior Alaska to explore how interactions between fire disturbance and other factors influence carbon storage of boreal forests. Below, we highlight important findings related to our understanding of the effects of fire on soil thermal and carbon dynamics of boreal forests.

### 4.1. Evaluation of Soil Thermal Dynamics

[46] While the patterns of soil temperature in 1997 were generally similar between model-based and field-based estimates, it is important to recognize that it was necessary to prescribe the pattern of moss growth through time and the depth of the humic organic layer in 1997 to produce the level of agreement in soil temperature. This was specifically highlighted by simulation for the stand that burned in 1996,

for which soil temperature was colder than in more recently burned stands because a substantial layer of humic organic matter remained after the fire. The sensitivity analyses that were focused on moss growth and fire severity verified that the growth of the moss and organic horizons after fire disturbance are important in the temporal dynamics of simulated soil temperature. It is well known that surface temperature decreases with the increasing thickness of moss and peat in high latitude ecosystems, and that variations in vegetation canopy per se have a relatively minor influence on the ground thermal regime compared to the surface organic layer [Brown, 1963, 1965, 1983; Riseborough, 1985; William and Smith, 1989]. Fire disturbance affects active layer dynamics of ecosystems underlain by permafrost by altering the insulation provided by moss and organic soil layers [Viereck, 1972, 1973, 1983; Rouse, 1976; Dyrness and Norum, 1983; Van Cleve et al., 1996; Yoshikawa et al., 2002]. The simulations that we conducted not only agree with these observations, but also suggest that there are important interactions between soil temperature and soil moisture dynamics. The sensitivity analyses in this study indicate that soil temperature is substantially affected by soil moisture during stand development.

### 4.2. Evaluation of Carbon Dynamics

[47] Similar to measurements of soil respiration reported for the fire chronosequence [O'Neill et al., 2002; see also O'Neill, 2000] and for an experimental burn near Fairbanks, Alaska (D. Valentine and R. D. Boone, unpublished data, 2001), our simulations indicate that soil respiration drops by approximately 50% immediately after fire. This is similar to observations in Canada [Burke et al., 1997; Wang et al., 2002]. The loss of root respiration associated with the mortality of vegetation in fire is the mechanism that is clearly responsible for this decline in the simulations that we conducted. While soil respiration declines substantially and immediately after fire, our simulations indicate that recently burned stands are losing carbon for approximately 30 to 60 years until the ecosystem starts accumulating carbon as NPP becomes greater than decomposition. The 30 to 60 year time period for carbon accumulation in our simulations contrasts with the 7- to 15-year time period from the application of a steady state model based on NPP and decomposition measurements for mature stands in the BOREAS region [Harden et al., 2000] (K. P. O'Neill et al., unpublished data, 2001). The timing of the transition from carbon source to carbon sink activity in the simulations of this study is similar to the findings of Rapalee et al. [1998] for stands developing after fire in the BOREAS region of Canada.

[48] Kasischke et al. [1995] hypothesized that decomposition in excess of carbon inputs to the soil lead to cumulative carbon losses after fire (prior to carbon accumulation), which is referred to by some as "postfire emissions," that are greater than carbon losses in fire emissions. Our sensitivity analysis for fire severity agrees with this hypothesis as decomposition in excess of inputs of carbon to the soil led to mean postfire carbon losses of 4330 g C m<sup>-2</sup> prior to carbon accumulation across the three scenarios, while mean losses in fire emissions were 1672 g C m<sup>-2</sup> across the three scenarios. This result agrees with the observations by Auclair and Carter [1993] that postfire carbon releases were approximately three times the

carbon released in fire emissions. Together, the scenarios of the three sensitivity analyses that we conducted indicate that postfire carbon losses are more sensitive to soil moisture levels and the amount of soil organic matter after fire (including inputs from fire-induced plant mortality) than to differences in soil temperature among scenarios. Preliminary data on the relationship of soil respiration to fire severity for an experimental burn near Fairbanks, Alaska [see *Burke et al.*, 1997] (Valentine and Boone, unpublished data, 2001) agree with the interpretation that the amount of soil organic matter plays a more important role in soil respiration responses after fire than does soil temperature. Thus, our simulations suggest that soil drainage and the effects of fire severity on the initial amount of soil organic matter after fire are more important than postfire soil temperature dynamics in the magnitude of "postfire emissions."

[49] After fire, soil carbon declines in our simulations because decomposition is higher than NPP and accumulates once inputs to the soil from NPP become greater than decomposition during stand development. In our sensitivity analyses, NPP drops to very low levels immediately after the fire, increases to a peak between 60 and 100 years after fire, and then declines to stabilize at a lower level in comparison to the peak. The accumulation of vegetation carbon storage follows the pattern of NPP. The pattern of NPP dynamics with stand age in our simulations is consistent with the pattern identified in other studies [*Buchmann and Schulze*, 1999; *Schulze et al.*, 2000; see also *Bonan and Van Cleve*, 1992; *McMurtrie et al.*, 1995]. In all of our analyses, the pattern of NPP closely followed the pattern of net nitrogen mineralization. Our simulated patterns of net nitrogen mineralization are similar to the patterns documented by *Smith et al.* [2000] for black spruce forests, in which rates in the organic horizons ranged from  $0.33 \text{ g N m}^{-2}$  in a recent burn to  $1.71 \text{ g N m}^{-2}$  from June to October in a mature black spruce forest. Analysis of our simulations indicated that the decline of NPP in older stands is proximately associated with declines in GPP, i.e., declines in photosynthesis. The decline in GPP is tied to lower nitrogen availability as net nitrogen mineralization declines because of lower organic matter quality with stand age, which is consistent with the nutrient availability hypothesis outlined by *McMurtrie et al.* [1995] and *Gower et al.* [1996]. The decline in NPP with stand age in our simulations is not consistent with the hypothesis that the decline is caused by increases in hydraulic resistance with stand age as the model does not explicitly consider hydraulic resistance. Also, the decline in NPP with stand age in our simulations is not consistent with the hypothesis of that the decline is caused by increases in autotrophic respiration with stand age, as autotrophic respiration in our simulations declines in older stands as declines in GPP drive declines in vegetation carbon.

[50] During the carbon accumulation phase of stand development, our sensitivity analyses indicated that carbon accumulation was affected by moss growth, soil moisture, and fire severity. While the effects of moss growth on soil temperature had little influence on the net rate of ecosystem carbon accumulation, moss growth affected the allocation of carbon storage. The lower soil temperature associated with the growth of moss caused lower decomposition and lower

net nitrogen mineralization, which led to higher rates soil carbon accumulation and lower rates of vegetation carbon accumulation, respectively. Soil moisture also affected allocation patterns of carbon storage in which higher soil moisture caused higher decomposition and higher net nitrogen mineralization, which led to lower rates of soil carbon accumulation and higher rates of vegetation carbon accumulation. It is important to recognize that this interpretation of the dynamics is limited to aerobic decomposition as we expect the opposite would occur when decomposition becomes more anaerobic. The results of the soil moisture sensitivity analysis and the sensitivity of soil carbon storage patterns to transient versus constant climate (Figures 10a and 10b) indicate that inter-annual and longer term variability in climate has the potential to interact with stand development to influence carbon storage [see also *Lynch and Wu*, 1999].

[51] In our simulations, fire severity also affected carbon accumulation patterns as the higher loss of nitrogen in more severe fires caused lower levels of NPP that led to lower accumulation of vegetation carbon and soil carbon. Similar to our simulations, it has been observed that NPP of larch forests in China is lower in severely burned stands than in lightly burned stands [*Wang et al.*, 2001]. Even though decomposition was lower for severely burned stands in our simulations, inputs to the soil from lower NPP were not able to replace higher levels of soil carbon lost in the fire. Furthermore, our sensitivity analysis for fire severity indicated that losses of carbon and nitrogen have the potential to influence carbon storage patterns during stand development more than changes in soil temperature and soil moisture. A number of studies have documented that fire can cause severe nitrogen losses from forests [*Dyrness et al.*, 1989; *Driscoll et al.*, 1999; *Grogan et al.*, 2000; *Smith et al.*, 2000; *Wan et al.*, 2001; but see *Brais et al.*, 2000]. The simulations in which we added nitrogen to replace nitrogen losses that occurred in fire emissions indicated that carbon storage was very sensitive to inputs of nitrogen during stand development after fire. Recent syntheses of the carbon costs and benefits of nitrogen fixation indicate that nitrogen fixation rates should change substantially during stand development after disturbance [*Rastetter et al.*, 2001]. We conclude that nitrogen fixation is an important process to represent in modeling decadal to century scale responses of carbon dynamics during stand development after fire disturbance.

## 5. Conclusion

[52] Many of our interpretations and conclusions concerning the temporal patterns of soil temperature, moss growth, soil moisture, and carbon dynamics from the application of the STM-TEM to the chronosequence in interior Alaska agree with the interpretations and conclusions from the empirical studies for the chronosequence [see *O'Neill*, 2000; *O'Neill et al.*, 2002]. The degree of agreement between the modeling and empirical studies gave us confidence in using the model as a tool to conduct sensitivity analyses that explored how the complexity of interactions among various factors influence carbon dynamics after fire disturbance in boreal forests. These sensitivity analyses indicated that along with differences in fire and

climate history, a number of other factors influence the response of carbon dynamics to fire disturbance. These factors include nitrogen fixation, the growth of moss, changes in the depth of the organic layer, soil drainage, and fire severity. While number studies have investigated how these factors influence the dynamics of boreal forests, our empirical and mechanistic understanding of how these factors influence ecosystem dynamics of boreal forests after disturbance is limited. The long timescales over which disturbance effects persist make monitoring changes and determining mechanisms responsible for changes difficult. The ability to conduct sensitivity analyses with the model to make specific predictions about the role of these factors during stand development presents the opportunity for testing the validity of the model mechanisms with well-designed field studies. Thus, the analyses in this study highlight the potential value of integrating field and modeling studies for clarifying how different factors influence ecosystem processes in boreal forests during stand development after fire disturbance.

## Appendix A: The Hydrological Model (HM)

### A1. State Variables and Fluxes

[53] The definition of state variables and fluxes for water are described in Figure 1b. The state equations for the HM are:

$$\frac{dR_t}{dt} = R_{Ft} - R_{THt} - E_{Ct} \quad (A1)$$

$$\frac{dS_t}{dt} = S_{Ft} - S_{THt} - S_{St} \quad (A2)$$

$$\frac{dG_S}{dt} = S_{THt} - S_{Mt} - GS_{St} \quad (A3)$$

$$\frac{dM_{MO}}{dt} = S_{Mt} + R_{THt} - P_{1t} - E_{Mt} - ROR_{MOt} - ROS_{MOt} \quad (A4)$$

$$\frac{dR_{DS}}{dt} = ROR_{MOt} - ROR_{DS} \quad (A5)$$

$$\frac{dS_{DS}}{dt} = ROS_{MOt} - ROS_{DS} \quad (A6)$$

$$\frac{dM_{HU}}{dt} = P_{1t} - P_{2t} - T_{C1t} \quad (A7)$$

$$\frac{dM_{MI}}{dt} = P_{2t} - T_{C2t} - D_{Rt} \quad (A8)$$

where  $t$  is the time step of the calculation (month). Units for all state variables are in mm and for all flux variables are in mm month<sup>-1</sup>.

[54] Below we describe the details for the calculation of each the fluxes simulated by the HM. See Table 2 for documentation of parameter values used in this study.

### A2. Rainfall and Snowfall

[55] Monthly air temperature ( $T$ , input data) partitions monthly precipitation (input data) into rainfall,  $R_F$  ( $T \geq$

$-1^\circ\text{C}$ ), or snowfall,  $S_F$  ( $T < -1^\circ\text{C}$ ) [Willmott et al., 1985].

### A3. Canopy Transpiration

[56] Canopy transpiration ( $T_C$ ) is similar to the formulation described by *Running and Coughlan* [1988]:

$$T_C = \frac{(R_{AC} \times \beta) \times (C_P \times \rho_A) \times V_D / \rho_A}{\beta + \gamma \times (1.0 + R_C / R_A)} \times \frac{D_L \times M_D}{\lambda_W \times 1000} \quad (A9)$$

where  $T_C$  is monthly canopy transpiration ( $\text{m}^3 \text{month}^{-1}$ ),  $\beta$  is the derivative of humidity deficit ( $\text{mbar } ^\circ\text{C}^{-1}$ ) at ambient mean monthly air temperature ( $T$ ),  $R_{AC}$  is mean monthly short wave radiation integrated through the canopy ( $\text{MJ m}^{-2} \text{d}^{-1}$ ),  $C_P$  is specific heat of air ( $\text{J kg}^{-1} \text{ } ^\circ\text{C}^{-1}$ ),  $\rho_A$  is density of air ( $\text{kg m}^{-3}$ ),  $V_D$  is vapor pressure deficit ( $\text{mbar}$ ),  $R_A$  is canopy aerodynamic resistance ( $\text{s m}^{-1}$ ),  $R_C$  is canopy resistance to water vapor,  $\gamma$  is psychrometric constant ( $\text{mbar } ^\circ\text{C}^{-1}$ ),  $\lambda_W$  is latent heat of vaporization of water ( $\text{MJ kg}^{-1}$ ),  $D_L$  is day length ( $\text{s d}^{-1}$ ), and  $M_D$  is the number of days per month.

[57] The mean radiation integrated through the canopy,  $R_{AC}$ , is calculated as:

$$R_{AC} = NIRR \times \frac{1.0 - e^{-(LAI/2.2) \times E_R}}{E_R \times LAI/2.2} \quad (A10)$$

where  $R_{AC}$  is in units of  $\text{MJ m}^{-2} \text{d}^{-1}$ ,  $NIRR$  ( $\text{MJ m}^{-2} \text{d}^{-1}$ ) is mean daily short-wave radiation at the top of the canopy as calculated by TEM,  $LAI$  is leaf area index ( $\text{m}^2 \text{m}^{-2}$ ) as calculated by TEM (see equation (5)), and  $E_R$  is a dimensionless extinction coefficient of radiation through the canopy.

[58] The derivative of humidity deficit,  $\beta$ , is calculated as a function of  $T$  and  $V_D$ :

$$\beta = V_D \times \frac{4098 + 34.5 \times T}{(237.3 + T)^2} \quad (A11)$$

[59] Mean monthly vapor pressure deficit,  $V_D$ , is calculated as a function of  $T$ :

$$V_D = 6.1078 \times e^{\frac{17.27 \times T}{237.3 + T}} \quad (A12)$$

[60] Canopy resistance to water vapor,  $R_C$ , is calculated as the inverse of canopy conductance,  $G$  ( $\text{m s}^{-1}$ ):

$$G = G_{\max} - DG_W \times (LWP - LWP_{\min}) \quad (A13)$$

where  $G_{\max}$  is maximum canopy conductance ( $\text{m s}^{-1}$ ),  $DG_W$  is the slope of  $G$  versus  $LWP$ ,  $LWP$  is the mean daily maximum leaf water potential across the month ( $-\text{MPa}$ ), and  $LWP_{\min}$  is the minimum leaf water potential inducing stomatal closure, defined here as the spring minimum  $LWP$  ( $-\text{MPa}$ ). Mean daily maximum leaf water potential across the month is calculated as:

$$LWP = \frac{0.2}{SOIL_w / SOIL_{cap}} \quad (A14)$$

where  $SOIL_w$  is mean monthly soil water content ( $m^3$ ) integrated across the humic organic and mineral soil layers, and  $SOIL_{cap}$  is a parameter for soil water capacity ( $m^3$ ) of the humic organic and mineral soil layers [see *Running and Coughlan*, 1988; *Frolking et al.*, 1996].

#### A4. Canopy Interception of Rain, Canopy Evaporation, and Throughfall of Rain

[61] Monthly canopy interception of rain ( $R_I$ ) is based on  $R_F$  and a parameter for the canopy interception of rainfall per unit rainfall ( $I_{RMAX}$ ) [*Helvey*, 1971; see also *Helvey and Patric*, 1965]. The potential interception of rain ( $PR_I$ ) is calculated as:

$$PR_I = R_F \times I_{RMAX} \quad (A15)$$

If  $R_F$  is less than  $PR_I$ ,  $R_I$  is equal to  $R_F$ ; otherwise,  $R_I$  is set up equal to  $PR_I$ . Monthly canopy evaporation ( $E_C$ ) is equal to  $R_I$ . Monthly throughfall of rain ( $R_{TH}$ ) is calculated as the difference between  $R_F$  and  $R_I$ .

#### A5. Canopy Interception of Snow, Throughfall of Snow, and Canopy Snow Sublimation

[62] Monthly canopy interception of snow ( $S_I$ ) is based on  $S_F$  and a parameter that defines the maximum daily interception of snow per unit leaf area ( $I_{SMAX}$ ,  $mm LAI^{-1} d^{-1}$ ) [*Coughlan and Running*, 1997]. The potential interception of snow ( $PS_I$ ) is calculated as:

$$PS_I = M_D \times LAI \times I_{SMAX} / 2.0 \quad (A16)$$

[63] If  $S_F$  is less than  $PS_I$ ,  $S_I$  is equal to  $S_F$ ; otherwise  $S_I$  is set up equal to  $PS_I$ . Monthly throughfall of snow ( $S_{TH}$ ) is calculated as the difference between  $S_F$  and  $S_I$ . Monthly canopy sublimation of snow ( $S_S$ ) is calculated based on  $S_I$  and potential sublimation of snow from the canopy ( $SUB_{CP}$ ). If  $S_I$  is less than  $SUB_{CP}$ , then  $S_S$  is equal to  $S_F$ . If  $S_I$  is greater than  $SUB_{CP}$  then  $S_S$  is equal to  $SUB_{CP}$ . The  $SUB_{CP}$  ( $mm month^{-1}$ ) is similar to the calculation by *Coughlan and Running* [1997]:

$$SUB_{CP} = \frac{RA_C \times 1000}{\lambda_W + K} \times M_D \quad (A17)$$

where  $\lambda_W$  is latent heat of vaporization of water ( $MJ mm^{-1} M^{-2}$ ) and  $K$  is latent heat fusion ( $MJ mm^{-1} M^{-2}$ ).

#### A6. Soil Surface Evaporation

[64] The potential soil surface evaporation ( $PE_M$ ,  $mm month^{-1}$ ) of daytime is based on the Penman equation [see *Monteith and Unsworth*, 1990; *Waring and Running*, 1998]:

$$PE_M = (E_{rate} + V_D \times 100 \times G_b / \psi) \times M_D \quad (A18)$$

where  $E_{rate}$  is the equilibrium evaporation rate ( $m s^{-1}$ ) of an extensive, homogeneous wet surface,  $V_D$  is the air saturation deficit (mbar),  $G_b$  is the soil surface boundary layer conductance for water vapor ( $m s^{-1}$ ) [*Grace*, 1981], and  $\psi$  is a function that depends on density of air, the gas constant for water vapor, and air temperature.

[65] The equilibrium evaporation rate ( $E_{rate}$ ) is based on [*McNaughton*, 1976]:

$$E_{rate} = \frac{\xi \times R_n}{\rho_A \times \lambda_W \times (\xi + 1.0)} \quad (A19)$$

where  $\xi$  is the change of latent heat relative to the change of sensible heat of saturated air,  $R_n$  is net irradiation ( $Wm^{-2}$ ) at the soil surface,  $\rho_A$  is the density of air. The variable  $\xi$  is 1.26 at  $10^\circ C$  and is calculated to increase exponentially with mean monthly temperature based on the calculations of *Dilly* [1968] and *Murray* [1967]:

$$\xi = 0.7185 \times e^{0.0544 \times T} \quad (A20)$$

$R_n$  is calculated as [*Coughlan and Running*, 1997]:

$$R_n = RA_c \times e^{-E_R \times LAI / 2.2} \quad (A21)$$

$\psi$  is based on the data of *McNaughton* [1976]:

$$\psi = \rho_A \times (\xi + 1.0) \times G_V \times T \quad (A22)$$

where  $G_V$  is the gas constant for water vapor ( $0.462 m^{-3} kPa kg^{-1} K^{-1}$ ). Similar to *Thornton* [2000], the monthly actual soil evaporation ( $E_M$ ,  $mm month^{-1}$ ) is based on the estimated dry and wet days. If  $R_{TH}$  is greater than or equal to  $PE_M$  within a month,  $E_M$  is estimated as:

$$E_M = 0.6 \times PE_M \quad (A23)$$

Otherwise, the  $E_M$  is estimated as the proportion of  $PE_M$ :

$$E_M = E_{VR} \times PE_M \quad (A24)$$

where  $E_{VR}$  is calculated as:

$$E_{VR} = \frac{0.3}{DSR^{2.0}} \quad (A25)$$

where  $DSR$  is the number of dry days in the month.  $DSR$  is estimated probabilistically as:

$$DSR = (1 - P_R) \times M_D \quad (A26)$$

where  $P_R$  is probability of rain days within a month.  $P_R$  is estimated as an empirical function of throughfall rain (E. B. Rastetter, unpublished data, 1989).

$$P_R = 1 - e^{-\mu \times R_{TH}} \quad (A27)$$

where  $\mu$  is a parameter.

#### A7. Snowmelt and Sublimation From Ground Snow Layer

[66] If  $S_{TH}$  is greater than 0 and  $T$  is above  $-1^\circ C$ , maximum monthly snowmelt ( $MS_M$ ) driven by incident radiation on the snow surface is based on the data of *Coughlan* [1991] as:

$$MS_M = M_D \times \alpha \times R_n / K \quad (A28)$$

where  $MS_M$  is in units  $\text{mm month}^{-1}$ ,  $\alpha$  is snow albedo. If  $MS_M$  is less than  $S_{TH}$ , then snowmelt ( $M_S$ ) is equal to  $MS_M$ , otherwise  $M_S$  is equal to  $S_{TH}$ . If air temperature is less than  $-1^\circ\text{C}$ ,  $M_S$  is 0, and potential sublimation ( $PGS_S$ ) from snow on the ground is calculated as:

$$PGS_S = M_D \times R_{SUB}/L_S \quad (\text{A29})$$

where  $PGS_S$  is in unit  $\text{mm month}^{-1}$ ;  $L_S$  is latent heat of sublimation ( $\text{KJ kg}^{-1}$ ), and  $R_{SUB}$  is a radiation-based variable that drives sublimation.  $R_{SUB}$  is calculated as:

$$R_{SUB} = R_n \times S_A \quad (\text{A30})$$

where parameter  $S_A$  is radiation absorptivity of snow ( $\text{KJ kg}^{-1}$ ). If  $S_{TH}$  is greater than  $PGS_S$ , then snow sublimation ( $GS_S$ ) is equal to  $PGS_S$ , otherwise  $GS_S$  is equal to  $S_{TH}$ .

### A8. Available Water Capacity, Percolation, and Drainage

[67] Available water capacity of each layer depends on field capacity and wilting point:

$$AWC_{MO} = FC_{MO} - WP_{MO} \quad (\text{A31})$$

$$AWC_{HU} = FC_{HU} - WP_{HU} \quad (\text{A32})$$

$$AWC_{MI} = FC_{MI} - WP_{MI} \quad (\text{A33})$$

where  $AWC_{MO}$ ,  $AWC_{HU}$ , and  $AWC_{MI}$  are parameters for available water capacity (mm),  $FC_{MO}$ ,  $FC_{HU}$ , and  $FC_{MI}$  are parameters for field capacity (mm), and  $WP_{MO}$ ,  $WP_{HU}$ , and  $WP_{MI}$  are parameters for wilting point (mm) of the moss plus fibric, humic organic, and mineral soil layers, respectively.

[68]  $FC_{MO}$ ,  $FC_{HU}$ ,  $FC_{MI}$ ,  $WP_{MO}$ ,  $WP_{HU}$ , and  $WP_{MI}$  are calculated as:

$$FC_{MO} = D_{moss} \times PFC_{MO} \times 10 \quad (\text{A34})$$

$$FC_{HU} = D_{HU} \times PFC_S \times 10 \quad (\text{A35})$$

$$FC_{MI} = D_{MI} \times PFC_S \times 10 \quad (\text{A36})$$

$$WP_{MO} = D_{moss} \times PWP_{MO} \times 10 \quad (\text{A37})$$

$$WP_{HU} = D_{HU} \times PWP_S \times 10 \quad (\text{A38})$$

$$WP_{MI} = D_{MI} \times PWP_S \times 10 \quad (\text{A39})$$

where  $D_{moss}$ ,  $D_{HU}$ , and  $D_{MI}$  are depths (m) of the moss plus fibric, humic organic, and mineral soil layers, respectively,  $PFC_{MO}$  and  $PWP_{MO}$  are field capacity (%) and wilting point (%) for moss plus fibric layer, and  $PFC_S$  and  $PWP_S$  are parameters for field capacity (%) and wilting point (%) for the soil.  $D_{moss}$  is either calculated dynamically (see equation (1)) or prescribed, while  $D_{HU}$  and  $D_{MI}$  are prescribed. The parameters  $PFC_S$  and  $PWP_S$  are calculated based on soil texture as in version 4.0 and 4.1 of TEM [McGuire et al., 1995, 1997; Tian et al., 1999]:

$$PFC_S = (PF_A \times P_{S+C}) + PF_B \quad (\text{A40})$$

$$PWP_S = (PW_A \times P_{S+C}) + PW_B \quad (\text{A41})$$

Where  $PF_A$ ,  $PF_B$ ,  $PW_A$ , and  $PW_B$  are parameters.  $P_{S+C}$  is calculated as a function of soil texture based on the percent of silt ( $PCT_{slt}$ ) and percent of clay ( $PCT_{clay}$ ) of the soil:

$$P_{S+C} = (PCT_{slt} + PCT_{clay}) \times 0.01 \quad (\text{A42})$$

[69] Percolation and drainage are calculated, in part, based on an empirical equation described by Neilson [1993, 1995] [see also Haxeltine, 1996; Pan et al., 2002]:

$$P_L = P_C \times \left( \frac{AW_L}{AW_{CL}} \right)^4 \times M_D \quad (\text{A43})$$

where  $P_L$  is the monthly percolation from the upper (L) to lower soil layer (L-1);  $P_C$  is the empirical percolation coefficient that depends on soil texture;  $AW_L$  is the available soil water in the upper soil layer (L),  $AW_{CL}$  is the available water holding capacity for the upper layer (L) that depends on the soil texture. When soil temperature of a soil layer is lower than  $0^\circ\text{C}$ , there is no percolation into the layer from the layer above and there is no percolation to the layer below; otherwise there is percolation based on equation (A43). While the above formulation is used to calculate percolation from the moss layer to the humic organic layer ( $P_1$ ), the formulation is used to make an initial estimates of percolation from the humic organic layer to the mineral soil layer ( $IP_2$ ), and the initial estimate of drainage from the mineral soil layer to groundwater ( $ID_R$ ). Percolation from the humic organic and mineral soil layers is calculated based on the initial estimates of percolation and excess percolation determined after available water is updated (see below).

[70] Available water of the moss plus fibric layer ( $AW_{MO}$ ) is updated monthly as:

$$AW_{MOt} = AW_{MOt-1} + S_M + R_{TH} - P_1 - E_M \quad (\text{A44})$$

If  $AW_{MO}$  is greater than  $AWC_{MO}$ , then runoff from the moss plus fibric layer is ( $RO_{MO}$ ,  $\text{mm month}^{-1}$ ) is calculated as:

$$RO_{MO} = AW_{MO} - AWC_{MO} \quad (\text{A45})$$

$RO_{MO}$  is partitioned to runoff derived from rainfall ( $ROR_{MO}$ ,  $\text{mm month}^{-1}$ ) and from snowmelt ( $ROS_{MO}$ ,  $\text{mm month}^{-1}$ ) as:

$$ROR_{MO} = \frac{S_M \times RO_{MO}}{R_{CH}} \quad (\text{A46})$$

$$ROS_{MO} = \frac{R_{TH} \times RO_{MO}}{R_{CH}} \quad (\text{A47})$$

where  $R_{CH}$  is recharge ( $\text{mm month}^{-1}$ ) calculated as:

$$R_{CH} = S_M + R_{TH} \quad (\text{A48})$$

[71] If the humic organic layer is within the active layer, then available water of the humic organic layer ( $AW_{HU}$ ) is updated as:

$$AW_{HUt} = AW_{HUt-1} + P_1 - T_{C1} - IP_2 \quad (\text{A49})$$

otherwise  $AW_{Hum}$  is equal to  $AW_{Hum-1}$ . If  $AW_{HU}$  is greater than  $AWC_{HU}$ , the excess water is forced to percolate to the mineral soil layer if the mineral soil layer is also within the active layer:

$$EP_{HU} = AW_{HU} - AWC_{HU} \quad (A50)$$

and percolation from the humic organic layer ( $P_2$ ) is calculated as the sum of  $IP_2$  and  $EP_{HU}$ .

[72] If the mineral soil layer is within the active layer, then available water of the mineral soil layer ( $AW_{MI}$ ) is updated monthly as:

$$AW_{MI} = AW_{MI-1} + P_2 - T_{C2} - ID_R \quad (A51)$$

otherwise  $AW_{MI}$  it equal to  $AW_{MI-1}$ . If  $AW_{MI}$  is greater than  $AWC_{MI}$ , the excess water is forced to drain to groundwater:

$$EP_{MI} = AW_{MI} - AWC_{MI} \quad (A52)$$

and drainage from the mineral soil layer ( $D_R$ ) is calculated as the sum of  $ID_R$  and  $EP_{MI}$ .

#### A9. Partitioning of Transpiration Between the Humic Organic and Mineral Soil Layers

[73] Canopy transpiration ( $T_C$ ) is split into  $T_{C1}$  and  $T_{C2}$ , based on the extraction rates of transpired water from the humic organic layer ( $\beta_1$ ) and mineral soil ( $\beta_2$ ) layer (i.e.,  $\beta_1 + \beta_2 = 1.0$ ), respectively:

$$T_{C1} = \beta_1 \times T_C \quad (A53)$$

$$T_{C2} = \beta_2 \times T_C \quad (A54)$$

The rates  $\beta_1$  and  $\beta_2$  are calculated as:

$$\beta_1 = \frac{AW_{HU}}{AW_{HU} + AW_{MI}} \quad (A55)$$

$$\beta_2 = \frac{AW_{MI}}{AW_{HU} + AW_{MI}} \quad (A56)$$

#### A10. Runoff

[74] Similar to the water balance model of *Vorosmarty et al.* [1989], whenever field capacity of the moss plus fibric layer is attained, the excess water is transferred to subsurface runoff pools for rainfall and snowmelt derived runoff as described above in equations (A43), (A44), and (A45). Runoff from the rainfall detention storage pool ( $ROR_{DS}$ , mm month<sup>-1</sup>) is calculated as:

$$ROR_{DS} = 0.5 \times (R_{DS} + C_P \times (R_{TH} + S_M - PET)) \quad (A57)$$

when  $M_{MO} = FC_{MO}$ ,  $R_{TH} + S_M \geq PET$

$$ROR_{DS} = 0.5 \times R_{DS} \quad \text{when } M_{MO} < FC_{MO} \text{ or } R_{TH} + S_M < PET \quad (A58)$$

where  $C_P$  is the proportion of surplus water attributable to rain ( $R_{TH}/[R_{TH} + S_M]$ ) and  $PET$  is potential evapotranspiration (mm month<sup>-1</sup>).

[75]  $PET$  is calculated based on the Jensen-Haise formulation [Jensen and Haise, 1963], which depends on  $T$  and radiation:

$$PET = \left[ 0.04 \times \left( \left( \frac{9.0}{5.0} \times T \right) + 32.0 \right) - 0.37 \right] \times NIRR \times 0.016742 \times M_D \quad (A59)$$

If  $PET$  is less than 0.0, then  $PET$  is set up to be 0. Estimated actual evapotranspiration (EET, mm month<sup>-1</sup>) is calculated based on the estimates of evaporation, sublimation, and transpiration as:

$$EET = S_S + GS_S + E_C + E_M + T_{C1} + T_{C2} \quad (A60)$$

[76] Runoff from the snowmelt detention storage pool ( $ROS_{DS}$ , mm month<sup>-1</sup>) depends on elevation. For sites at elevations of 500 m or below,  $ROS_{DS}$  is equal to 10% of  $S_{DS}$  pool in the first month of snowmelt. In subsequent months, these sites will lose 50% of  $S_{DS}$  per month. At higher elevations, sites will lose 10% of  $S_{DS}$  in the first month, followed by 25% in the second month and 50% thereafter.

#### A11. Volumetric Soil Moisture and Water-Filled Pore Space

[77] Some formulations in TEM require volumetric soil moisture (VSM), while others require percent water-filled pore space (WFPS). Estimates of VSM for each of the soil layers are calculated from the state variables  $M_{MO}$ ,  $M_{HU}$ ,  $M_{MI}$  as:

$$VSM_{MO} = \frac{M_{MO}}{D_{MOSS}} \times 0.1 \quad (A61)$$

$$VSM_{HU} = \frac{M_{HU}}{D_{HU}} \times 0.1 \quad (A62)$$

$$VSM_{MI} = \frac{M_{MI}}{D_{MI}} \times 0.1 \quad (A63)$$

where  $VSM_{MO}$ ,  $VSM_{HU}$ , and  $VSM_{MI}$  are volumetric soil moisture (%) for three soil layers, respectively. In equations (A61)–(A63), the factor 0.1 is used to convert to percent as  $M_{MO}$ ,  $M_{HU}$ , and  $M_{MI}$  are in mm and  $D_{MOSS}$ ,  $D_{HU}$ , and  $D_{MI}$  are in m.

[78] Estimates of WFPS for each of the soil layers are calculated from the state variables  $M_{MO}$ ,  $M_{HU}$ ,  $M_{MI}$  as:

$$WFPS_{MO} = \frac{M_{MO}}{POR_{MO}} \quad (A64)$$

$$WFPS_{HU} = \frac{M_{HU}}{POR_{HU}} \quad (A65)$$

$$WFPS_{MI} = \frac{M_{MI}}{POR_{MI}} \quad (A66)$$

where  $WFPS_{MO}$ ,  $WFPS_{HU}$ , and  $WFPS_{MI}$  are percent of pore space, and  $POR_{MO}$ ,  $POR_{HU}$ , and  $POR_{MI}$  are pore space (mm) for moss plus fibric organic, humic organic, and mineral soil layers, respectively.

[79]  $POR_{MO}$  is estimated as:

$$POR_{MO} = D_{MOSS} \times MO_{PO} \times 10 \quad (A67)$$

where parameter  $MO_{PO}$  is the porosity of moss plus fibric layer (%).

[80]  $POR_{HU}$  and  $POR_{MI}$  are calculated as:

$$POR_{HU} = D_{HU} \times PCT_{PO} \times 10 \quad (A68)$$

$$POR_{MI} = D_{MI} \times PCT_{PO} \times 10 \quad (A69)$$

[81]  $PCT_{PO}$  is calculated as:

$$PCT_{PO} = PCT_{POA} \times P_{S+C} + PCT_{POB} \quad (A70)$$

where  $PCT_{POA}$  and  $PCT_{POB}$  are parameters.

[82] **Acknowledgments.** The senior author thanks Larry Hinzman for insightful discussions about the hydrological aspects of research represented in this paper. We also thank Terry Chapin for valuable comments on previous drafts of this manuscript. This research was supported by the NASA Land Cover and Land Use Change Program (NAG5-6275), the USGS Geologic Division Global Change Research Program, the NSF Taiga Long Term Ecological Research Program (DEB-9810217), the NSF Arctic System Science and Arctic Natural Science Programs (OPP-9614253, OPP-9732126, OPP-9870635), and the Alaska Cooperative Fish and Wildlife Research Unit.

## References

- Aguado, E., Radiation balances of melting snow covers at an open site in the central Sierra Nevada, California, *Water Resour. Res.*, 21, 1034–1049, 1985.
- Amthor, J. S., et al., Boreal forest CO<sub>2</sub> exchange and evapotranspiration predicted by nine ecosystem process models: Inter-model comparisons and relations to field measurements, *J. Geophys. Res.*, 106, 33,623–33,648, 2001.
- Atjay, G. L., P. Ketner, and P. DuVignaud, Terrestrial primary production and phytomass, in *The Global Carbon Cycle*, edited by B. E. Bolin et al., vol. 13, pp.129–181, John Wiley, New York, 1977.
- Auclair, A. N. D., and T. B. Carter, Forest wildfires as a recent source of CO<sub>2</sub> at northern latitudes, *Can. J. For. Res.*, 23, 1528–1536, 1993.
- Barber, V. A., G. P. Juday, and B. P. Finney, Reduced growth of Alaska white spruce in the twentieth century from temperature-induced drought stress, *Nature*, 405, 668–673, 2000.
- Beltrami, H., and J. C. Mareschal, Ground temperature changes in eastern Canada: Borehole temperature evidence compared with proxy data, *Terra Nova*, 5, 21–28, 1994.
- Bonan, G. B., and K. VanCleve, Soil temperature, nitrogen mineralization, and carbon source-sink relationships in boreal forests, *Can. J. For. Res.*, 22, 629–639, 1992.
- Brais, S., P. David, and R. Ouimet, Impacts of wild fire severity and salvage harvesting on the nutrient balance of jack pine and black spruce boreal stands, *For. Ecol. Manage.*, 137, 231–243, 2000.
- Brown, R. J. E., Influence of vegetation on permafrost, in *Proceedings, Permafrost International Conference, Publ. 1287*, pp. 20–25, NAS/NRC, Washington D. C., 1963.
- Brown, R. J. E., Some observations on the influence of climatic and terrain features on permafrost at Norman Wells, N.W.T., *Can. J. Earth Sci.*, 2, 15–31, 1965.
- Brown, R. J. E., Effects of fire on the permafrost ground thermal regime, in *The Role of Fire in Northern Circumpolar Ecosystems*, edited by R. W. Wein and D. A. MacLean, pp. 97–110, John Wiley, New York, 1983.
- Buchmann, N., and E. Schulze, Net CO<sub>2</sub> and H<sub>2</sub>O fluxes of terrestrial ecosystems, *Global Biogeochem. Cycles*, 13, 751–760, 1999.
- Burke, R. A., R. G. Zepp, M. A. Tarr, W. L. Miller, and B. J. Stocks, Effect of fire on soil-atmosphere exchange of methane and carbon dioxide in Canadian boreal forest sites, *J. Geophys. Res.*, 102, 29,289–29,300, 1997.
- Chapin, F. S., III, and E. Mathews, Boreal carbon pools: Approaches and constraints in global extrapolations, in *Carbon Cycling in Boreal Forests and Sub-Arctic ecosystems*, edited by T. S. Vinson and T. P. Kolchugina, pp. 9–20, U.S. Dept. of Commer., Washington, D. C., 1993.
- Clein, J. S., B. L. Kwiatkowski, A. D. McGuire, J. E. Hobbie, E. B. Rastetter, J. M. Melillo, and D. W. Kicklighter, Modeling carbon responses of tundra ecosystems to historical and projected climate: A comparison of a fine- and coarse-scale ecosystem model for identification of process-based uncertainties, *Global Change Biol.*, 6(suppl. 1), 127–140, 2000.
- Clein, J. S., A. D. McGuire, X. Zhang, D. W. Kicklighter, J. M. Melillo, S. C. Wofsy, and P. G. Jarvis, The role of nitrogen dynamics in modeling historical and projected carbon balance of mature black spruce ecosystems across North America: Comparisons with CO<sub>2</sub> fluxes measured in the Boreal Ecosystem Atmosphere Study (BOREAS), *Plant Soil*, 242, 15–32, 2002.
- Coughlan, J. C., and S. W. Running, Regional ecosystem simulation: A general model for simulating snow accumulation and melt in mountainous terrain, *Landscape Ecol.*, 12, 119–136, 1997.
- Coughlan, J. C., Biophysical aggregation of a forested landscape using a knowledge-based model, Ph.D. thesis, 111 pp., Univ. of Montana, Missoula, Mont., 1991.
- De Grandpre, L., L. Gagnon, and Y. Bergeron, Changes in the understorey of Canadian southern boreal forest after fire, *J. Veg. Sci.*, 4, 803–810, 1993.
- Dilley, A. C., On the computer calculation of vapor pressure and specific humidity gradients from psychrometric data, *J. Appl. Meteorol.*, 7, 717–719, 1968.
- Driscoll, K. G., J. M. Arocena, and H. B. Massicotte, Post-fire soil nitrogen content and vegetation composition in Sub-boreal spruce forests of British Columbia's central interior, Canada, *For. Ecol. Manage.*, 121, 227–237, 1999.
- Dymess, C. T., and R. A. Norum, The effects of experimental fires on black spruce forest floors in interior Alaska, *Can. J. For. Res.*, 13, 879–893, 1983.
- Dymess, C. T., K. Van Cleve, and J. D. Levison, The effect of wildfire on soil chemistry in four forest types in interior Alaska, *Can. J. For. Res.*, 19, 1389–1396, 1989.
- Flannigan, M. D. F., and C. E. Van Wagner, Climate change and wildfire in Canada, *Can. J. For. Res.*, 21, 66–72, 1991.
- French, N. H. F., et al., Controls on patterns of biomass burning in Alaskan boreal forests, in *Fire, Climate Change, and Carbon Cycling in the North American Boreal Forest*, *Ecol. Stud. Ser.*, vol. 138, edited by E. S. Kasischke and B. J. Stocks, pp. 148–163, Springer-Verlag, New York, 2000.
- Frolking, S., et al., Modelling temporal variability in the carbon balance of a spruce/moss boreal forest, *Global Change Biol.*, 2, 343–366, 1996.
- Gorham, E., Northern peatlands: Role in the carbon cycle and probable responses to climatic warming, *Ecol. Appl.*, 1, 182–195, 1991.
- Goulden, M. L., B. C. Daube, S. M. Fan, D. J. Sutton, A. Bazzaz, J. W. Munger, and S. C. Wofsy, Physiological responses of black spruce forest to weather, *J. Geophys. Res.*, 102, 28,987–28,996, 1997.
- Goulden, M. L., et al., Sensitivity of boreal forest carbon balance to soil thaw, *Science*, 279, 210–217, 1998.
- Gower, S. T., R. E. McMurtrie, and D. Murty, Aboveground net primary productivity decline with stand age: Potential causes, *Tree*, 11, 378–382, 1996.
- Gower, S. T., J. G. Vogel, J. M. Norman, C. J. Kucharik, S. J. Steele, and T. K. Stow, Carbon distribution and aboveground net primary production in aspen, jack pine, and black spruce stands in Saskatchewan and Manitoba, Canada, *J. Geophys. Res.*, 102, 29,029–29,041, 1997.
- Grace, J. C., Some effects of wind on plants, in *Plants and Their Atmospheric Environment*, edited by J. Grace, E. D. Ford, and P. G. Jarvis, pp. 31–56, Blackwell, Malden, Mass., 1981.
- Grogan, P., T. D. Bruns, and F. S. Chapin III, Fire effects on ecosystem nitrogen cycling in a California bishop pine forest, *Oecologia*, 122, 537–544, 2000.
- Harden, J. W., K. P. O'Neill, S. E. Trumbore, H. Veldhuis, and B. J. Stocks, Moss and soil contributions to the annual net carbon flux of a maturing boreal forest, *J. Geophys. Res.*, 102, 28,805–28,816, 1997.
- Harden, J. W., T. Fries, and T. Huntington, *Mississippi Basin Carbon Project—Upland Soil Database for Northwestern Mississippi*, *Open-file Rep. 98-440*, U.S. Geol. Surv., Menlo Park, Calif., 1998.
- Harden, J. W., S. E. Trumbore, B. J. Stocks, A. Hirsch, S. T. Gower, K. P. O'Neill, and E. S. Kasischke, The role of fire in the boreal carbon budget, *Global Change Biol.*, 6(suppl. 1), 174–184, 2000.
- Haxeltine, A., Modeling the vegetation of the Earth, Ph.D. thesis, 124 pp., Lund Univ., Sweden, 1996.
- Helvey, J. D., A summary of rainfall interception by certain conifers of North America, in *Proceedings of the Third International Symposium for Hydrology Professors Biological Effects in the Hydrological Cycle*, edited by E. J. Monke, pp. 103–113, Purdue Univ., West Lafayette, Ind., 1971.
- Helvey, J. D., and J. H. Patric, Canopy and litter interception by hardwoods of eastern United States, *Water Resour. Res.*, 1, 193–206, 1965.

- Hess, J. C., C. A. Scott, G. L. Hufford, and M. D. Fleming, El Nino and its impact on fire weather conditions in Alaska, *Int. J. Wildland Fire*, 10, 1–13, 2001.
- Jarvis, P. G., The interpretation of the variations in leaf water potential and stomatal conductance found in canopies in the field, *Philos. Trans. R. Soc. London, Ser. B*, 273, 593–610, 1976.
- Jarvis, P. G., and J. B. Moncrieff, The CO<sub>2</sub> Exchanges of Boreal Black Spruce Forest, in *Collected Data of The Boreal Ecosystem-Atmosphere Study* [CD-ROM], edited by J. Newcomer et al., NASA, Greenbelt, Md., 2000.
- Jensen, M. E., and H. R. Haise, Estimating evapotranspiration from solar radiation, *J. Irrig. Drain. Div., Am. Soc. Civ. Eng.*, 4, 15–41, 1963.
- Kasischke, E. S., N. L. Christensen, and B. J. Stocks, Fire, global warming, and the carbon balance of boreal forests, *Ecol. Appl.*, 5, 437–451, 1995.
- Kasischke, E. S., K. P. O'Neill, N. H. F. French, and L. L. Borgeau-Chavez, Controls on patterns of biomass burning in Alaskan boreal forests, in *Fire, Climate Change, and Carbon Cycling in the North American Boreal Forest*, *Ecol. Stud. Ser.*, vol. 138, edited by E. S. Kasischke and B. J. Stocks, pp.148–163, Springer-Verlag, New York, 2000.
- Kurz, W. A., and M. J. Apps, Retrospective assessment of carbon flows in Canadian boreal forests, in *Forest Ecosystems, Forest Management and the Global Carbon Cycle*, *NATO Adv. Sci. Inst. Ser.*, edited by M. J. Apps and D. T. Price, Springer-Verlag, New York, 1995.
- Kurz, W. A., and M. J. Apps, A 70-year retrospective analysis of carbon fluxes in the Canadian forest sector, *Ecol. Appl.*, 9, 56–547, 1999.
- Kurz, W. A., M. J. Apps, B. J. Stocks, and W. J. A. Volney, Global climate change: Disturbance regions and tropospheric feedbacks of temperate and boreal forests, in *Biotic Feedbacks in the Global Climate System*, edited by G. M. Woodwell and F. T. Makenzie, pp.119–133, Oxford Univ. Press, New York, 1995.
- Lachenbruch, A. H., and B. V. Marshall, Changing climate: Geothermal evidence from permafrost in the Alaskan Arctic, *Science*, 234, 689–696, 1986.
- Landsberg, J. J., *Physiological Ecology of Forest Production*, Academic, San Diego, Calif., 1986.
- Luc, L., and S. Luc, Vegetation changes caused by recent fires in the northern boreal forest of eastern Canada, *J. Veg. Sci.*, 9, 483–492, 1998.
- Lynch, A. H., and W. Wu, Impacts of fire and warming on ecosystem uptake in the boreal forest, *J. Clim.*, 13, 2334–2338, 1999.
- Lynham, T. J., G. M. Wickware, and J. A. Mason, Soil chemical changes and plant succession following experimental burning in immature jack pine, *Can. J. Soil Sci.*, 78, 93–104, 1998.
- McGuire, A. D., and J. E. Hobbie, Global climate change and the equilibrium responses of carbon storage in arctic and subarctic regions, in *Modeling the Arctic System: A Workshop Report on the State of Modeling in the Arctic System Science Program*, pp. 53–54, The Arctic Res. Consortium of the U.S., Fairbanks, Alaska, 1997.
- McGuire, A. D., J. M. Melillo, D. W. Kicklighter, and L. A. Joyce, Equilibrium responses of soil carbon to climate change: Empirical and process-based estimates, *J. Biogeogr.*, 22, 785–796, 1995.
- McGuire, A. D., J. M. Melillo, D. W. Kicklighter, Y. Pan, X. Xiao, J. Helfrich, B. Moore III, C. J. Vorosmarty, and A. L. Schloss, Equilibrium responses of global net primary production and carbon storage to doubled atmospheric carbon dioxide: Sensitivity to changes in vegetation nitrogen concentration, *Global Biogeochem. Cycles*, 11, 173–189, 1997.
- McGuire, A. D., J. M. Melillo, J. T. Randerson, W. J. Parton, M. Heimann, R. A. Meier, J. S. Clein, D. W. Kicklighter, and W. Sauf, Modeling the effects of snowpack on heterotrophic respiration across northern temperate and high latitude regions: Comparison with measurements of atmospheric carbon dioxide in high latitudes, *Biogeochemistry*, 48, 91–114, 2000a.
- McGuire, A. D., J. Clein, J. M. Melillo, D. W. Kicklighter, R. A. Meier, C. J. Vorosmarty, and M. C. Serreze, Modeling carbon responses of tundra ecosystems to historical and projected climate: The sensitivity of pan-arctic carbon storage to temporal and spatial variation in climate, *Global Change Biol.*, 6, S141–S159, 2000b.
- McGuire, A. D., et al., Carbon balance of the terrestrial biosphere in the twentieth century: Analyses of CO<sub>2</sub>, climate and land-use effects with four process-based ecosystem models, *Global Biogeochem. Cycles*, 15, 183–206, 2001.
- McMurtrie, R., E. S. T. Gower, M. G. Ryan, and J. J. Landsberg, Forest productivity: Explaining its decline with stand age, *Bull. Ecol. Soc. Am.*, 76, 152–154, 1995.
- McNaughton, K. G., Evaporation and advection, I, Evaporation from extensive homogeneous surfaces, *Q. J. R. Meteorol. Soc.*, 102, 81–191, 1976.
- McNaughton, K. G., and P. G. Jarvis, Predicting effects of vegetation changes on transpiration and evaporation, in *Water Deficit and Plant Growth*, edited by T. T. Kozlowski, vol. 7, pp. 1–47, Academic, San Diego, Calif., 1983.
- Melillo, J. M., D. W. Kicklighter, A. D. McGuire, W. T. Peterjohn, and K. M. Newkirk, Global change and its effects on soil organic carbon stocks, in *Role of Nonliving Organic Matter in the Earth's Carbon Cycle*, edited by R. G. Zepp and C. Sonntag, pp. 175–189, John Wiley, New York, 1995.
- Monteith, J. L., *Principles of Environmental Physics*, Edward Arnold, London, 1973.
- Monteith, J. L., and M. H. Unsworth, *Principles of Environmental Physics*, 2nd ed., Edward Arnold, London, 1990.
- Mosteller, F., R. E. K. Rourke, and G. B. Thomas Jr., *Probability With Statistical Applications*, Addison-Wesley, Reading, Mass., 1961.
- Murphy, P. J., B. J. Stocks, E. S. Kasischke, D. Barry, M. E. Alexander, N. H. F. French, and J. P. Mudd, Historical fire records in the North American boreal forest, in *Fire, Climate Change and Carbon Cycling in North American Boreal Forests*, *Ecol. Stud. Ser.*, vol. 138, edited by E. S. Kasischke and B. J. Stocks, pp. 274–288, Springer-Verlag, New York, 2000.
- Murray, F. W., On the computation of saturation vapor pressure, *J. Appl. Meteorol.*, 6, 203–204, 1967.
- Neilson, R. P., Vegetation redistribution: A possible biosphere source of CO<sub>2</sub> during climate change, *Water Air Soil Pollut.*, 70, 659–673, 1993.
- Neilson, R. P., A model for predicting continental scale vegetation distribution and water balance, *Ecol. Appl.*, 5, 362–386, 1995.
- Newcomer, J., et al. (Eds.), *Collected Data of The Boreal Ecosystem-Atmosphere Study* [CD-ROM], NASA, Greenbelt, Md., 2000.
- Oechel, W. C., and K. Van Cleve, The role of bryophytes in nutrient cycling in the taiga, in *Forest Ecosystems in the Alaskan Taiga*, edited by K. Van Cleve et al., pp. 121–137, Springer-Verlag, New York, 1986.
- Oechel, W. C., and G. L. Vourlitis, The effects of climate change on land-atmosphere feedbacks in arctic tundra regions, *Trends Ecol. Evol.*, 9, 324–329, 1994.
- O'Neill, K. P., Changes in carbon dynamics following wildfire in soils of interior Alaska, Ph.D. thesis, Duke Univ., Durham, N. C., 2000.
- O'Neill, K. P., E. S. Kasischke, and D. D. Richter, Seasonal and decadal patterns of soil carbon uptake and emission along an age-sequence of burned black spruce stands in interior Alaska, *J. Geophys. Res.*, 107, doi:10.1029/2001JD000443, in press, 2002.
- Osterkamp, T. E., and V. E. Romanovsky, Evidence for warming and thawing of discontinuous permafrost in Alaska, *Permafrost Periglacial Processes*, 10(1), 17–37, 1999.
- Pan, Y., A. D. McGuire, J. M. Melillo, D. W. Kicklighter, S. Sitch, and I. C. Prentice, A biogeochemistry-based successional model and its application along a moisture gradient in the continental United States, *J. Vegetation Sci.*, 13, 369–382, 2002.
- Post, W. M., W. R. Emanuel, P. J. Zinke, and A. G. Stangenberger, Carbon pools and world life zones, *Nature*, 298, 156–159, 1982.
- Potter, C. S., et al., Comparison of boreal ecosystem model sensitivity to variability in climate and forest site parameters, *J. Geophys. Res.*, 106, 33,671–33,688, 2001.
- Randerson, J. T., M. V. Thompson, T. J. Conway, I. Y. Fung, and C. B. Field, The contribution of terrestrial sources and sinks to trends in the seasonal cycle of atmospheric carbon dioxide, *Global Biogeochem. Cycles*, 11, 535–560, 1997.
- Rapalee, G., S. E. Trumbore, E. A. Davidson, J. W. Harden, and H. Veldhuis, Estimating soil carbon stocks and fluxes in a boreal forest landscape, *Global Biogeochem. Cycles*, 12, 687–701, 1998.
- Rastetter, E. B., P. M. Vitousek, C. Field, G. R. Shaver, D. Herbert, and G. I. Agren, Resource optimization and symbiotic nitrogen fixation, *Ecosystems*, 4, 369–388, 2001.
- Riseborough, D. W., Modeling climatic influences on permafrost at a boreal forest site, unpublished M.A. thesis, 172 pp., Carleton Univ., Ottawa, 1985.
- Rouse, W. R., Microclimatic changes accompanying burning in sub-arctic lichen woodland, *Arct. Alp. Res.*, 8, 357–376, 1976.
- Running, S. W., and J. C. Coughlan, A general model of forest ecosystem processes for regional applications, I, Hydrologic balance, canopy gas exchange and primary production processes, *Ecol. Modell.*, 42, 125–154, 1988.
- Ryan, M. G., A simple method for estimating gross carbon budgets for vegetation in forest ecosystems, *Tree Physiol.*, 9, 255–266, 1991.
- Ryan, M. G., D. Binkley, and J. H. Fownes, Age-related decline in forest productivity: Pattern and process, *Adv. Ecol. Res.*, 7, 213–262, 1996.
- Ryan, M. G., M. B. Lavigne, and S. T. Gower, Annual carbon cost of autotrophic respiration in boreal forest ecosystems in relation to species and climate, *J. Geophys. Res.*, 102, 28,871–28,883, 1997.
- Schimmel, J., and A. Granstrom, Fire severity and vegetation response in the boreal Swedish forest, *Ecology*, 77, 1436–1450, 1996.
- Schulze, E. D., C. Wirth, and M. Heimann, Managing forests after Kyoto, *Science*, 289, 2058–2059, 2000.

- Sellers, P. J., et al., BOREAS in 1997: Experiment overview, scientific results, and future directions, *J. Geophys. Res.*, 102, 28,731–28,769, 1997.
- Serreze, M. C., J. E. Walsh, F. S. Chapin III, T. Osterkamp, M. Dyurgerov, V. Romanovsky, W. C. Oechel, J. Morison, T. Zhang, and R. G. Barry, Observational evidence of recent change in the northern high-latitude environment, *Clim. Change*, 46, 159–207, 2000.
- Smith, C. K., M. R. Coyea, and A. D. Munson, Soil carbon, nitrogen, and phosphorus stocks and dynamics under disturbed black spruce forests, *Ecol. Appl.*, 10, 775–788, 2000.
- Stocks, B. J., M. A. Fosberg, M. B. Wotton, T. J. Lynham, and K. C. Ryan, Climate change and forest fire activity in North American boreal forests, in *Fire, Climate Change, and Carbon Cycling in the North American Boreal Forest*, edited by E. S. Kasischke and B. J. Stocks, pp. 312–319, Springer-Verlag, New York, 2000.
- Thic, J., Distribution and thawing of permafrost in the southern part of the discontinuous permafrost zone in Manitoba, *Arctic*, 27, 189–200, 1974.
- Thornton, P. E., *Biome-BGC version 4.1.1*, Numer. Terradyn. Simul. Group (NTSG), Sch. of For., Univ. of Mont., Missoula, Mont., 2000.
- Tian, H., J. M. Melillo, D. W. Kicklighter, A. D. McGuire, and J. Helfrich, The sensitivity of terrestrial carbon storage to historical climate variability and atmospheric CO<sub>2</sub> in the United States, *Tellus, Ser. B*, 51, 414–452, 1999.
- Trumbore, S. E., and J. W. Harden, Accumulation and turnover of carbon in organic and mineral soils of the BOREAS northern study area, *J. Geophys. Res.*, 2, 28,816–28,830, 1997.
- Van Cleve, K., C. T. Dyrness, L. A. Viereck, J. Fox, F. S. Chapin III, and W. Oechel, Taiga ecosystems in interior Alaska, *Bioscience*, 33(1), 39–44, 1983.
- Van Cleve, K., L. A. Viereck, and C. T. Dyrness, State factor control of soil and forest succession along the Tanana river in interior Alaska, U.S.A., *Arct. Alp. Res.*, 28, 388–400, 1996.
- Viereck, L. A., Ecological effects of river flooding and forest fires on permafrost in the taiga of Alaska, *Permafrost, North Am. Contrib. Int. Conf.*, 2nd, 60–67, 1972.
- Viereck, L. A., Wildfire in the taiga of Alaska, *Quat. Res.*, 3, 465–495, 1973.
- Viereck, L. A., The effects of fire in black spruce ecosystems of Alaska and northern Canada, in *The Role of Fire in Northern Circumpolar Ecosystems (Scope 18)*, edited by R. W. Wein and D. A. MacLean, pp. 132–145, John Wiley, New York, 1983.
- Vorosmarty, C. J., B. J. Peterson, E. B. Rastetter, and P. A. Steudler, Continental scale models of water balance and fluvial transport: An application to South America, *Global Biogeochem. Cycles*, 3, 241–265, 1989.
- Wan, S., D. Hui, and Y. Luo, Fire effects on nitrogen pools and dynamics in terrestrial ecosystems: A meta-analysis, *Ecol. Appl.*, 11, 1349–1365, 2001.
- Wang, C., S. T. Gower, Y. Wang, H. Zhao, P. Yan, and B. P. Bond-Lamberty, The influence of fire on carbon distribution and net primary production of boreal *Larix gmelinii* forests in north-eastern China, *Global Change Biol.*, 7, 719–730, 2001.
- Wang, C., B. P. Bond-Lamberty, and S. T. Gower, Soil surface CO<sub>2</sub> flux in boreal black spruce fire chronosequence, *J. Geophys. Res.*, 107, doi:10.1029/2001JD000861, in press, 2002.
- Waring, R. H., and S. W. Running, *Forest Ecosystems, Analysis at Multiple Scales*, 2nd ed., pp. 370, Academic, San Diego, Calif., 1998.
- Wardle, D. A., O. Zackrisson, and M.-C. Nilsson, The charcoal effect in Boreal forests: Mechanisms and ecological consequences, *Oecologia*, 115, 419–426, 1998.
- Weber, M. G., and K. Van Cleve, Nitrogen transformations in feather moss and forest floor layers of interior Alaska black spruce ecosystems, *Can. J. For. Res.*, 14, 278–290, 1984.
- Williams, P. J., and M. W. Smith, *The Frozen Earth, Fundamentals of Geocryology*, pp. 306, Cambridge Univ. Press, New York, 1989.
- Willmott, C. J., C. M. Rowe, and Y. Mintz, Climatology of the terrestrial seasonal water cycle, *J. Clim.*, 5, 589–606, 1985.
- Wotton, B. M., and M. D. Flannigan, Length of the fire season in a changing climate, *For. Chron.*, 69, 187–192, 1993.
- Yarie, J., and S. Billings, Carbon balance of the Taiga forest within Alaska, *Can. J. For. Res.*, 32, 757–767, 2002.
- Yoshikawa, K., W. R. Bolton, V. E. Romanovsky, M. Fukuda, and L. D. Hinzman, Impacts of wildfire on the permafrost in the boreal forests of interior Alaska, *J. Geophys. Res.*, 107, doi:10.1029/2001JD000438, in press, 2002.
- Zackrisson, O., Influence of forest fires on the North Swedish boreal forest, *Oikos*, 29, 22–32, 1977.
- Zhuang, Q., V. E. Romanovsky, and A. D. McGuire, Incorporation of a permafrost model into a large-scale ecosystem model: Evaluation of temporal and spatial scaling issues in simulating soil thermal dynamics, *J. Geophys. Res.*, 106, 33,649–33,670, 2001.
- Zimov, S. A., S. P. Davidov, G. M. Zimova, A. I. Davidova, F. S. Chapin, M. C. Chapin III, and J. F. Reynolds, Contribution of disturbance to increasing seasonal amplitude of atmospheric CO<sub>2</sub>, *Science*, 284, 1973–1976, 1999.
- Zoltai, S. C., Cyclic development of permafrost in the peatlands of north-western Alberta, Canada, *Arct. Alp. Res.*, 25, 240–246, 1993.

J. W. Harden, U.S. Geological Survey ms 962, 345 Middlefield Rd., Menlo Park, CA 94025, USA.

A. D. McGuire, U.S. Geological Survey, Alaska Cooperative Fish and Wildlife Research Unit, University of Alaska Fairbanks, Fairbanks, AK 99775, USA.

K. P. O'Neill, Forest Inventory & Analysis, North Central Research Station, USDA Forest Service, 1992 Folwell Ave., St. Paul, MN 55108, USA.

V. E. Romanovsky, Geophysical Institute, University of Alaska Fairbanks, Fairbanks, AK 99775, USA.

J. Yarie, Department of Forest Science, University of Alaska Fairbanks, Fairbanks, AK 99775, USA.

Q. Zhuang, The Ecosystems Center, Marine Biological Laboratory, 7 MBL Street, Woods Hole, MA 02543, USA. (qzhuang@mbl.edu)